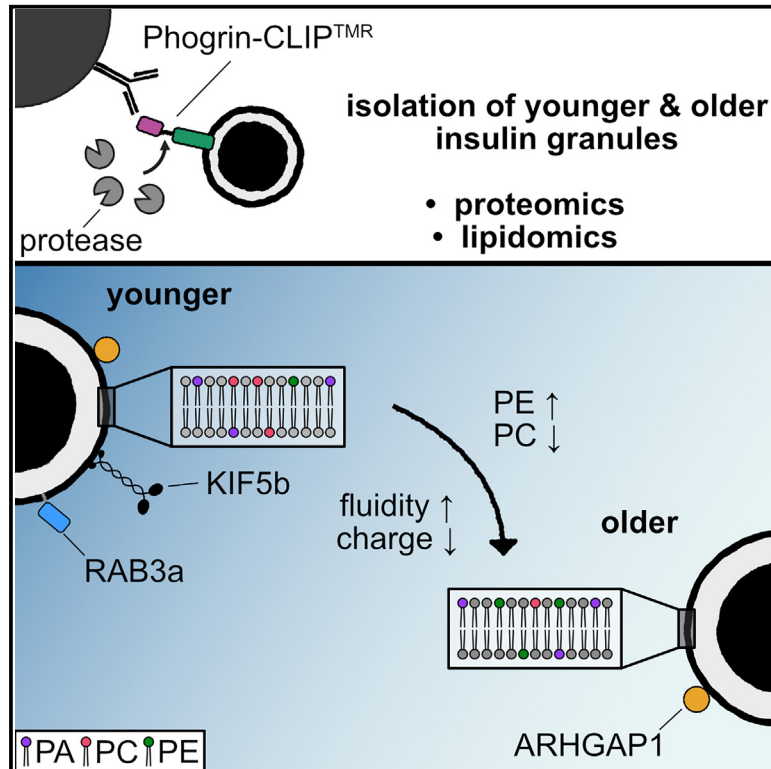


Purification of time-resolved insulin granules reveals proteomic and lipidomic changes during granule aging

Graphical abstract



Authors

Martin Neukam, Pia Sala, Andreas-David Brunner, ..., Matthias Mann, Ünal Coskun, Michele Solimena

Correspondence

mneukam@stanford.edu (M.N.), michele.solimena@uniklinikum-dresden.de (M.S.)

In brief

Neukam et al. employ a pulse-chase labeling approach to separate younger and older insulin secretory granules. Mass spectrometry identified RAB3a and KIF5b to be enriched on younger granules and ARHGAP1 on granules in general. The granule membrane PC/PE ratio, fluidity, and charge changed during aging from younger to older granules.

Highlights

- Development of a protocol for the isolation of age-defined insulin secretory granules (SGs)
- Proteomics reveals small GTPases and motor proteins associated with SGs of different age
- Lipidomics indicates phospholipid, membrane fluidity, and charge changes during SG aging



Article

Purification of time-resolved insulin granules reveals proteomic and lipidomic changes during granule aging

Martin Neukam,^{1,2,3,8,*} Pia Sala,^{2,3,4} Andreas-David Brunner,⁵ Katharina Ganß,^{1,2,3} Alessandra Palladini,^{2,3,4} Michal Grzybek,^{2,3,4} Oleksandra Topcheva,^{1,2,3} Jovana Vasiljević,^{1,2,3} Johannes Broichhagen,^{6,9} Kai Johnsson,⁶ Thomas Kurth,⁷ Matthias Mann,⁵ Ünal Coskun,^{2,3,4} and Michele Solimena^{1,2,3,10,*}

¹Molecular Diabetology, University Hospital and Faculty of Medicine Carl Gustav Carus, TU Dresden, 01307 Dresden, Germany

²Paul Langerhans Institute Dresden (PLID) of the Helmholtz Center Munich at the University Hospital Carl Gustav Carus and Faculty of Medicine of the TU Dresden, 01307 Dresden, Germany

³German Center for Diabetes Research (DZD), 85764 Neuherberg, Germany

⁴Center of Membrane Biochemistry and Lipid Research, University Hospital and Faculty of Medicine Carl Gustav Carus, TU Dresden, 01307 Dresden, Germany

⁵Max Planck Institute of Biochemistry, 82152 Martinsried, Germany

⁶Department of Chemical Biology, Max Planck Institute for Medical Research, 69120 Heidelberg, Germany

⁷TU Dresden, Center for Molecular and Cellular Bioengineering (CMCB), Technology Platform, Electron Microscopy and Histology Facility, 01307 Dresden, Saxony, Germany

⁸Present address: Department of Developmental Biology, Stanford University School of Medicine, Stanford, CA 94305, USA

⁹Present address: Leibniz-Forschungsinstitut für Molekulare Pharmakologie, 13125 Berlin, Germany

¹⁰Lead contact

*Correspondence: mneukam@stanford.edu (M.N.), michele.solimena@uniklinikum-dresden.de (M.S.)

<https://doi.org/10.1016/j.celrep.2024.113836>

SUMMARY

Endocrine cells employ regulated exocytosis of secretory granules to secrete hormones and neurotransmitters. Secretory granule exocytosis depends on spatiotemporal variables such as proximity to the plasma membrane and age, with newly generated granules being preferentially released. Despite recent advances, we lack a comprehensive view of the molecular composition of insulin granules and associated changes over their lifetime. Here, we report a strategy for the purification of insulin secretory granules of distinct age from insulinoma INS-1 cells. Tagging the granule-resident protein phogrin with a cleavable CLIP tag, we obtain intact fractions of age-distinct granules for proteomic and lipidomic analyses. We find that the lipid composition changes over time, along with the physical properties of the membrane, and that kinesin-1 heavy chain (KIF5b) as well as Ras-related protein 3a (RAB3a) associate preferentially with younger granules. Further, we identify the Rho GTPase-activating protein (ARHGAP1) as a cytosolic factor associated with insulin granules.

INTRODUCTION

Exocytosis is a fundamental cellular process to transport cargoes out of cells and to maintain plasma membrane (PM) protein and lipid homeostasis. Coordinated secretion in time and space is further crucial for the maintenance of extracellular matrix and cell-cell communication. In addition to constitutive exocytosis, which is constantly occurring in all cells, specialized professional secreting cells employ regulated exocytosis. Here, a specific trigger is required to elicit secretion of vesicles awaiting exocytosis upon elevation of intracellular Ca^{2+} levels. This pathway is utilized by many cell types, including neuropeptide-secreting neurons and peptide-hormone-secreting endocrine cells. Among the latter, pancreatic islet β cells require stimulation by glucose or other secretagogues to secrete insulin.

Like other cargoes undergoing regulated exocytosis, insulin is produced as an inactive prohormone precursor in the endo-

plasmic reticulum (ER) and delivered via the Golgi apparatus to immature insulin secretory granules (SGs), also known as (large) dense core vesicles. Activation of prohormone convertases upon acidification of the immature SG lumen drives the conversion of proinsulin into insulin and, thereby, SG maturation. Mature insulin SGs are then stored in the cytoplasm until hyperglycemia triggers their exocytosis for insulin release.

Insulin SGs are not equally competent for exocytosis but are categorized into functionally distinct pools. SGs close to the PM are considered more likely to undergo exocytosis.^{1,2} In addition to their location, SG age plays an important role, with newly synthesized insulin SGs having a greater propensity for exocytosis compared with older ones,^{3–6} a feature β cells share with many other cell types showing regulated exocytosis.^{7–12} Aging of SGs correlates with a change of their characteristics; at least in the case of insulin SGs of rat insulinoma INS-1 cells, younger SGs are more mobile and acidic relative to aged SGs^{13,14}—two



properties that might contribute to their preferential release. At the same time, older SGs are increasingly removed by autophagy/crinophagy.^{15,16} Alternative protocols using timer proteins suggested that, prior to this process, older SGs have decreased directed mobility,^{17,18} underscoring the need to investigate the molecular signatures of SGs of distinct age. Proteins or lipids involved in this age-specific behavior, however, are not yet known.

Progress in the proteomic and lipidomic characterization of age-distinct SG pools has been hampered by the lack of protocols for their purification, with recent efforts exploring the use of flow cytometry.¹⁹ Previous approaches isolating insulin SGs for proteomics analysis have led to the identification of 51–140 SG proteins, including many established cargoes and several new candidates.^{20–22} However, technical limitations could not prevent the co-enrichment of non-SG proteins, while several well-known SG transmembrane proteins and luminal cargoes were not detected.²³ Typical enrichment protocols for organelles are prone to cross-contamination, which reduces the accuracy of downstream proteomics and lipidomics analyses. The most widely applied method for organelle purification is subcellular fractionation, either by differential or gradient centrifugation. Both procedures, however, cannot avoid the co-enrichment of other cellular compartments, especially vesicular organelles with similar physical properties, such as lysosomes, synaptic-like microvesicles, or endosomes. A notable exception has been the purification of neuronal synaptic vesicles from brain synaptosomes to homogeneity, which has been possible largely due to the very high abundance of these organelles.^{24,25} An alternative is the immunoisolation of organelles with antibodies recognizing the cytoplasmic domain of a transmembrane bait protein followed by the binding of the antibody to an affinity matrix.^{26–28} Since copies of post-Golgi apparatus vesicle transmembrane proteins are also in transit through the ER and the Golgi apparatus at the time of cell lysis, contamination by the latter organelles is nonetheless likely.

Here we report an immunobased approach for the purification of insulin SGs of distinct age. Our protocol takes advantage of the specificity of immunopurification and combines it with pulse-chase labeling to restrict the antigen to post-Golgi apparatus organelles using a cleavable CLIP tag. We show that our approach dramatically reduces background, giving access to highly purified SGs that can be eluted as intact organelles. Notably, this approach is further suitable for the isolation of age-distinct insulin SG pools. We analyzed the proteomics and phospholipidomics profiles of younger and older SGs from INS-1 cells. Our data indicate that the ratio of phosphatidylcholine to phosphatidylethanolamine changes during SG aging, which affects the fluidity and charge of SG membranes *in vitro*. We further identified a preferential association of the motor protein KIF5b and RAB3a with younger SGs as well as ARHGAP1 with SGs in general.

RESULTS

Strategy

Immunopurification protocols provide high specificity for the respective antigen but often suffer from contamination by pull-

down of other organelles and unspecific binding to magnetic beads. To address those shortcomings, we fused the CLIP tag to the cytoplasmic C terminus of phogrin, an intrinsic membrane protein of SGs, also known as PTPRN2 or IA2-beta²⁹ (Figure 1A). CLIP is a self-labeling protein tag that can covalently bind to a cell-permeable CLIP substrate³⁰ (such as benzylcytosine [BC]-tetramethylrhodamine [TMR] or BC-fluorescein) in a pulse-chase manner, thereby ensuring that only newly synthesized phogrin-CLIP is labeled. Cells are then incubated until labeled phogrin-CLIP exits the Golgi apparatus and is sorted into immature SGs (Figure 1B), which then typically evolve into mature SGs within ~2 h.³¹ Varying the time interval between the labeling of newly synthesized phogrin-CLIP and cell lysis, it is possible to obtain extracts in which only a time-resolved pool of SGs contains the labeled phogrin-CLIP bait.

Using an antibody directed against the CLIP substrate, such as the fluorescent dye TMR or fluorescein (Fluo), rather than against the bait protein allows both the purification of age-distinct SGs and the exclusion of contaminants from pre-SG compartments along the secretory pathway. To reduce background by non-specific binding to the magnetic beads, we further included a human rhinovirus (HRV) 3C protease cleavage site between the CLIP tag and the cytoplasmic domain of phogrin, enabling the specific elution of the immunisolated organelles from the beads (Figure 1A). We chose phogrin as a bait protein specific to SGs because its cytosolic tail, unlike that of its paralog, islet cell autoantigen 512^{32,33} (ICA512; also known as PTPRN or IA-2), has not been reported to be proteolytically cleaved by calpain upon its transient insertion into the PM³⁴ and thereby to be potentially depleted in older SGs following repeated rounds of kiss-and-run or partial exocytosis. Hence, phogrin is an optimal candidate for the cytoplasmic addition of a CLIP tag at its C terminus. Since phogrin has been proposed to have phosphatidylinositol phosphatase activity,³⁵ we further replaced its catalytic cysteine 931 with serine³⁵ to avoid interference by overexpression of our reporter. Addition of the CLIP tag not only allows the age-distinct purification of SGs but also restricts the antigen (the CLIP label) to post-Golgi apparatus compartments.

Microscopic and biochemical characterization of phogrin-CLIP

First, we tested the subcellular localization of phogrin-CLIP C931S (hereafter called phogrin-CLIP) to ensure its efficient and specific targeting to insulin SGs. Super-resolution microscopy revealed that phogrin-CLIP covalently labeled with the dye BC-TMR was found in punctate structures that almost exclusively co-localized with endogenous insulin (Figures 1C and 1D). We did not detect significant co-localization with the early endosomal and lysosomal markers early endosome antigen 1 (EEA1) and lysosome-associated membrane glycoprotein 2 (LAMP2; Figures 1D, S1B, and S1C). Co-labeling for CLIP with an antibody served as a positive control (Figures 1D and S1A) and revealed that not all fusion proteins were positive for TMR; i.e., that washes after the labeling pulse were sufficient to prevent continuous labeling (Figure S1A).

We also analyzed some of the properties of a stable phogrin-CLIP INS-1 cell line. As expected, we could not detect the CLIP

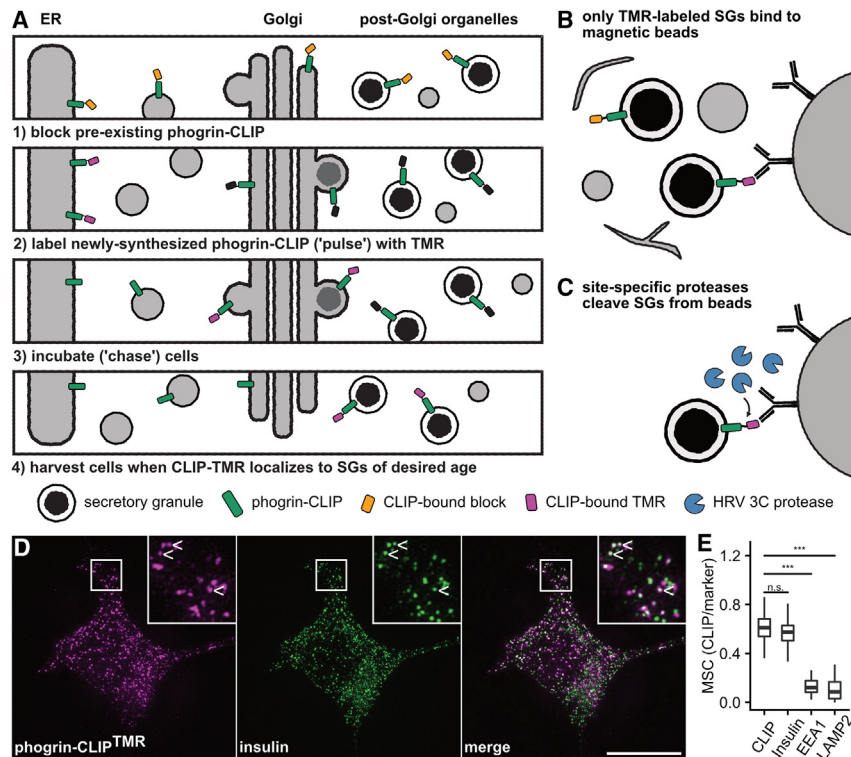


Figure 1. Generation and subcellular localization of phogrin-CLIP

(A) Schematic illustrating the pulse-chase labeling strategy used to purify SGs of distinct age. (1) All pre-existing phogrin-CLIP is blocked with saturating concentrations of BC-block. (2) Newly synthesized phogrin-CLIP localizes to the ER and is labeled or "pulsed" with BC-TMR. (3) In a "chase" period, cells are incubated until phogrin-CLIP^{TMR} travels along the secretory pathway past the Golgi apparatus. (4) When phogrin-CLIP^{TMR} localizes to SGs (of desired age), cells are harvested.

(B) Cell homogenates are incubated with anti-TMR antibodies. Only TMR/antibody-labeled SGs are bound to antibody-binding magnetic beads.

(C) Washing removes other organelles and membranes, and a site-specific HRV 3C protease cleaves intact SGs from the magnetic beads.

(D) Representative SIM image of an INS-1 cell stably expressing phogrin-CLIP labeled with CLIP-Cell TMR-Star and co-stained for insulin. Scale bar: 10 μ m.

(E) Quantification of co-localization of phogrin-CLIP labeled with TMR and various markers. Anti-CLIP antibodies served as a positive control. Co-localization was calculated using the Manders split coefficient (MSC). Data are represented as boxplots with median \pm SD. Statistical analysis corresponds to t test; *** $p < 0.001$. n.s., not significant. Cells from three independent experiments ($n = 24$ – 32) were analyzed.

signal in non-transfected control samples but only in the stable cell line (Figure S2A). Addition of the \sim 20-kDa CLIP tag retarded the electrophoretic mobility of prophogrin by SDS-PAGE to an apparent molecular weight of \sim 120 kDa and that of the converted, mature phogrin to \sim 80 kDa (Figure S2A). Probing for untagged phogrin, we found that the stably expressing phogrin-CLIP INS-1 cells retained the expression of endogenous phogrin like control cells, as shown by real-time PCR and immunoblot (Figures S2A and S2B). Since tagging of phogrin has been shown previously to affect insulin granule size, mobility, and exocytosis,³⁶ we tested whether phogrin-CLIP overexpression affected the levels of other insulin SG components and insulin secretion in our clone. Compared with non-transfected INS-1 cells, phogrin-CLIP INS-1 cells did not display obvious changes in the content of chromogranin A (CHGA), prohormone convertase 2 (PC2), or carboxypeptidase E (CPE), as shown by immunoblot (Figure S2C). However, stable overexpression of phogrin-CLIP correlated with increased glucose-stimulated insulin secretion, whereas insulin biosynthesis was unaffected (Figures S2D and S2E).

We further assessed the N-glycosylation status of phogrin-CLIP to verify its maturation and trafficking. Rat and mouse phogrin are predicted to be N-glycosylated at N553 and N550, respectively. Digestion with endoglycosidase H (EndoH), which only cleaves the N-glycan chain prior to its modification in the *cis*-Golgi apparatus, did not change the electrophoretic mobility of prophogrin-CLIP but affected an intermediate species (Figure S2F). In contrast, digestion with peptide:N-glycosidase F (PNGaseF), which removes all N-glycans, accelerated the electrophoretic mobility of all phogrin-CLIP species, consistent with being originally N-glycosylated (Figure S2F). Hence, mature

phogrin-CLIP and prophogrin-CLIP, but not an intermediate species, were insensitive to treatment with EndoH (Figure S2F). These data indicate that phogrin-CLIP progresses as expected along the secretory pathway.

Next, we transfected the stable phogrin-CLIP line with our previously described human insulin-SNAP (Ins-SNAP) reporter for SG aging⁶ to test whether the two reporters have similar localization and SG aging kinetics. When the CLIP and SNAP tags were simultaneously labeled with the orthogonal dyes BC-TMR and SNAP-Cell 430, respectively, for an SG age of 2–4 h, we could detect a high level of correlation (Figures S3A–S3C). However, the signals of 20- to 22 h-old Ins-SNAP⁴³⁰ and 2- to 4-h-old phogrin-CLIP^{TMR} were clearly distinct and not significantly correlated (Figures S3B and S3C).

Taken together, we conclude that phogrin-CLIP is transferred efficiently to the Golgi apparatus and post-Golgi apparatus and that its stable overexpression does not significantly alter insulin SG stores. It also has kinetics similar to Ins-SNAP and can serve as a reliable bait for the immunopurification of age-distinct insulin SG pools.

Immunopurification of phogrin-CLIP and SGs

Despite the use of specific antibodies, immunopurification protocols often suffer from non-specific co-enrichment. This is due to non-specific binding of the antibodies as well as unintended absorption of proteins to the solid phase, such as magnetic beads, during the isolation procedure. To reduce such background, we incorporated a site-specific protease cleavage site into phogrin-CLIP (Figure 1A), allowing the selective elution of the SGs from the beads. Using silver staining after SDS-PAGE,

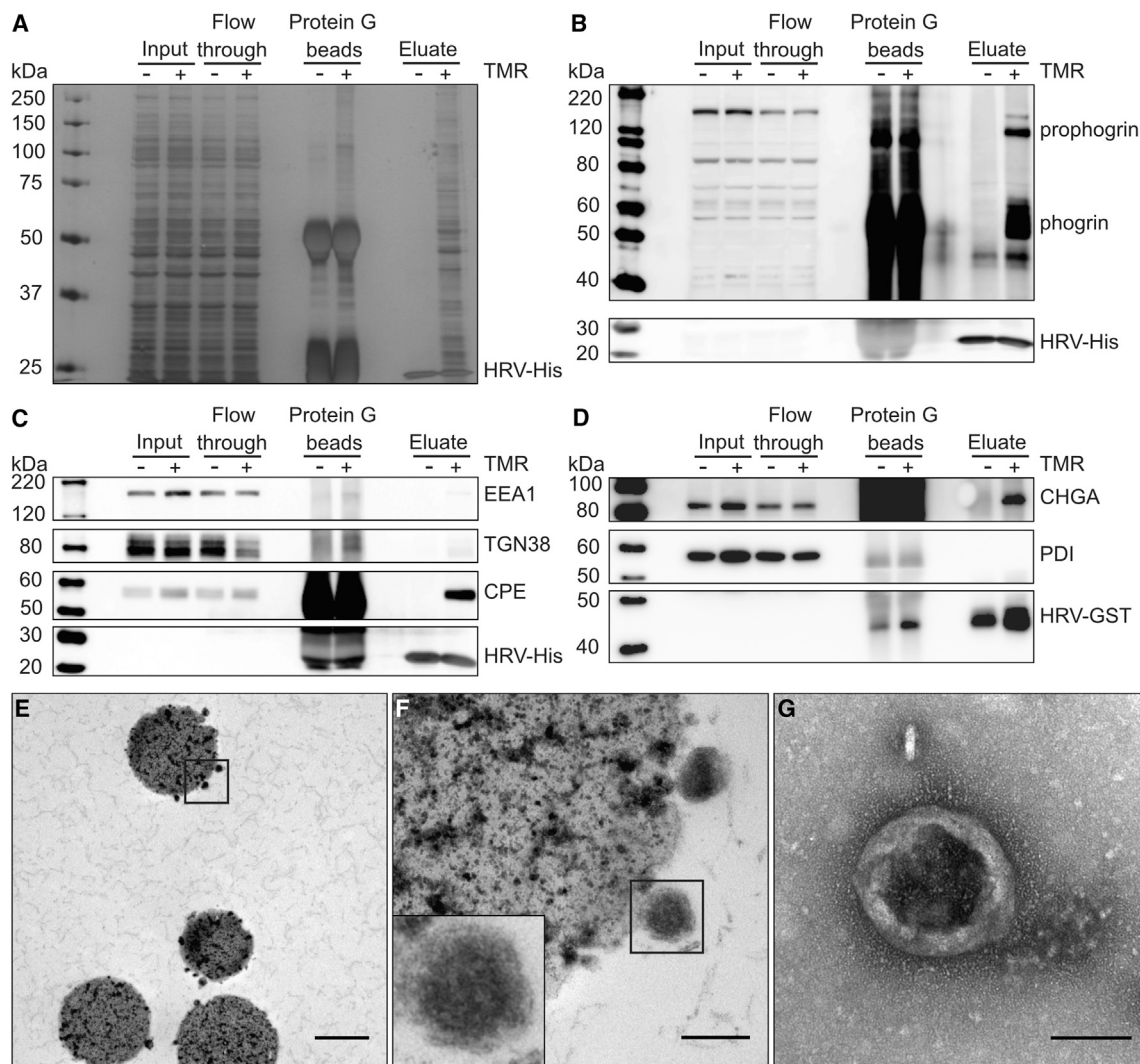


Figure 2. Characterization of SG enrichment purity

(A) Silver staining of material enriched from cells labeled with or without CLIP-Cell TMR-Star. Input (10 μ g), flowthrough (10 μ g) and protein G bead fractions were loaded for comparison. The added protease is visible at \sim 25 kDa.

(B) Material from SG purification was loaded and probed for phogrin by western blot.

(C and D) (C) SGs were purified and analyzed by western blot for the organelle markers EEA1, TGN38, and CPE or (D) CHGA and PDI. The His- or GST-tagged HRV 3C protease (HRV-His or -GST) in the eluate served as a loading control.

(E–G) Ultrastructural analysis of purified insulin SGs by electron microscopy.

(E) Micrograph of a bead sample prior to the addition of the HRV 3C protease embedded in Epon.

(F) Micrograph of the inset in (E).

(G) Negative staining of eluted material from specific samples as shown in (E) and (F).

Scale bars: 1 μ m (E), 200 nm (F), and 100 nm (G).

we assessed the degree of background of immunisolated labeled and unlabeled samples. As expected, the input and flow-through in both TMR-positive and -negative samples appeared similar (Figure 2A) and showed a plethora of bands. Similarly, beads from both samples showed distinct protein bands, which, however, were slightly more abundant in the TMR-positive samples. The eluates, released from the beads by addition of the protease, were instead remarkably different. Apart from a distinct band of \sim 25 kDa, representing the added protease,

no protein was visible in the eluate of the beads incubated with the unlabeled phogrin-CLIP control sample. In contrast, the eluate of the beads incubated with the TMR-labeled phogrin-CLIP sample showed a multitude of protein bands (Figure 2A).

To verify the selective immunisolation and elution of SGs, we immunoblotted control and labeled fractions for markers of distinct intracellular compartments. In contrast to the control sample, the eluate from the TMR-labeled phogrin-CLIP sample was enriched for several SG cargoes, including CPE, PC2,

CHGA, ICA512, and phogrin (Figures 2B–2D and S4A–S4C). It was negative instead for the Golgi apparatus markers trans-Golgi network integral membrane protein 38 (TGN38) and 130 kDa cis-Golgi matrix protein (GM130), the ER markers calnexin (CANX) and protein disulfide-isomerase (PD; Figures 2C, 2D, S4A, and S4B), as well as the early endosome marker EEA1 (Figure 2C). We could also detect the immature SG marker islet cell autoantigen 69^{37,38} (ICA69; Figure S4A). As expected from the silver staining, none of the mentioned markers were present in the eluate from the control beads. We could, however, detect the lysosomal marker LAMP2 and the synaptic-like microvesicle marker synaptophysin 1 (SYP1; Figure S4D). To limit contamination by these organelles, we included an immunodepletion step with antibodies targeting the cytoplasmic tails of either LAMP2 alone or both LAMP2 and SYP1. Both proteins could be depleted with the anti-LAMP2 antibody alone, suggesting that both markers resided in a common organelle (Figure S4E).

Finally, we evaluated the ultrastructural integrity of the purified SGs by transmission electron microscopy. To this aim, either beads of TMR-labeled samples were embedded in Epon for imaging of ultrathin sections (Figures 2E and 2F), or eluted SGs were directly spotted on grids for negative staining (Figure 2G). Electron micrographs confirmed the purity and integrity of the immunisolated SGs with no obvious contamination from other organelles. Epoxy-embedded SGs bound to beads contained the characteristic dense core of insulin SGs surrounded by a lipid bilayer (Figure 2F). In summary, these data indicate that our protocol allows the highly specific and background-low enrichment of insulin SGs from INS-1 cells using a cytoplasmic CLIP tag.

Lipidomic analysis of isolated insulin SGs

Having established that our protocol is suitable for the purification of SGs with high purity, we isolated SGs for shotgun lipid mass spectrometry (MS). For isolation of SGs without age bias, we labeled the cells without the addition of a blocking substrate, thereby labeling all pre-existing SGs (termed “mixed”). To investigate potential differences in lipid profiles of younger and older SGs, we first labeled phogrin-CLIP with an additional blocking step to saturate all existing CLIPs (Figure 1B). We then labeled newly synthesized phogrin-CLIP with BC-Fluo and incubated the cells until labeled phogrin-CLIP reached the desired age: 1–4 h for younger SGs and 16.5–22 h for older SGs.

Given the overall low amount of sample available for MS, we were able to identify, with high certainty, ~100 different lipid species (Tables S1 and S2). When analyzing the data by principal-component analysis, we found that samples from younger SGs clustered well together and separately from the similarly clustered older SGs, whereas mixed samples were scattered in between (Figure 3A).

Phosphatidylcholine (PC), phosphatidylethanolamine (PE), and phosphatidylserine (PS) were the most abundant lipid species (Figure 3B). We further detected considerable amounts of diacylglycerol (DAG) and phosphatidic acid (PA). Minor fractions of phosphatidylinositol (PI) and sphingomyelin (SM), as well as negligible amounts of ceramide (Cer) and phosphatidylglycerol (PG) were present (Figure 3B). Purified SGs showed compositional differences with a higher fraction of PC in younger and PE in older SGs (Figure 3B). Most of the lipids were unsaturated with either

one double bond ($46.7\% \pm 2.67\%$ vs. $36.53\% \pm 2.90\%$ for younger and older SGs, respectively) or two double bonds ($28.53\% \pm 2.81\%$ vs. $26.14\% \pm 1.25\%$ for younger and older SGs, respectively; Figure 3C). Only $12.03\% \pm 2.12\%$ and $23.48\% \pm 2.10\%$ of the lipids were fully saturated in younger and older SGs, respectively (Figure 3C). The overall length distribution favored chain lengths of 32, 34, and 36 carbons and a smaller fraction of 38 (Figure 3D). Taken together, older SGs contained a higher fraction of lipids with higher saturation and shorter acyl chain length (Figures 3C and 3D). We analyzed the 10 most abundant lipid species for potential changes between younger and older SGs. In older SGs, PE 32:0 was more abundant, whereas younger SGs contained more PC 32:1, 34:1, 34:2, and 36:2 (Figure 3E).

Given these differences in lipid composition, we tested whether they are sufficient to alter the biophysical properties of the membranes; namely, membrane fluidity and charge. To do so, we prepared liposomes from lipid extracts of isolated SGs in which the fluorescent C-Laurdan probe was introduced to measure the general polarization (GP) index.³⁹ Liposomes formed from lipids of younger SGs were more rigid than those of older SGs, as evidenced by their higher GP values (Figure 3F). In addition, we found that liposomes from lipids of younger SGs were more negatively charged than those from lipids of older SGs (Figure 3G). Notably, the composition of mixed SGs had intermediate lipidomic (Figures 3B–3E) and GP or zeta values (Figures 3F and 3G), presumably reflecting a true mixture of younger and older SGs.

In summary, the lipidomes of younger and older SGs revealed a change of the PC/PE ratio during the granule aging process, accompanied by an *in vitro* change of the biophysical properties of their membranes.

Proteomics analysis of isolated insulin SGs

To characterize the protein composition of our purified SGs, we labeled SGs as described above and examined the eluted material by MS. First, we purified total SGs without age bias and analyzed their proteome in comparison with control samples without labeling (Tables S3 and S4). Like the analyses by silver staining after gel electrophoresis and by western blot, we found that the unlabeled samples contained significantly fewer proteins than the labeled fractions (Figures 4A and 4B). The 299 proteins identified in unlabeled fractions were among the 1,010 proteins present in labeled fractions, and no protein exclusive to unlabeled samples was identified (Figures 4A and 4B). Significantly enriched were 8 and 875 proteins in the unlabeled and labeled fractions, respectively (Figure 4A; Table S4). In the labeled fractions, we could identify most known SG proteins, such as CPE, ICA512, phogrin, INS1/2, PC1/3 and PC2, islet amyloid polypeptide (IAPP), and vesicle-associated membrane protein 2 (VAMP2; also known as synaptobrevin-2) and subunits of the vacuolar H⁺-ATPase (Figure 4A). However, despite pre-clearing, lysosomal contaminants, such as LAMP1/2 and cathepsin A/B, could still be detected (Figure S5A). Additionally, markers of endosomes (RAB7a and RAB11) and mitochondria (voltage-dependent anion-selective channel protein 2 [VDAC2] and ATP synthase subunit alpha, mitochondrial [ATP5a1]) were present.

Similar to the lipidomic profiling, we analyzed the proteomes of younger and older SGs (Tables S5 and S6). Unbiased principal-component analysis indicated that, also on the proteomics level,

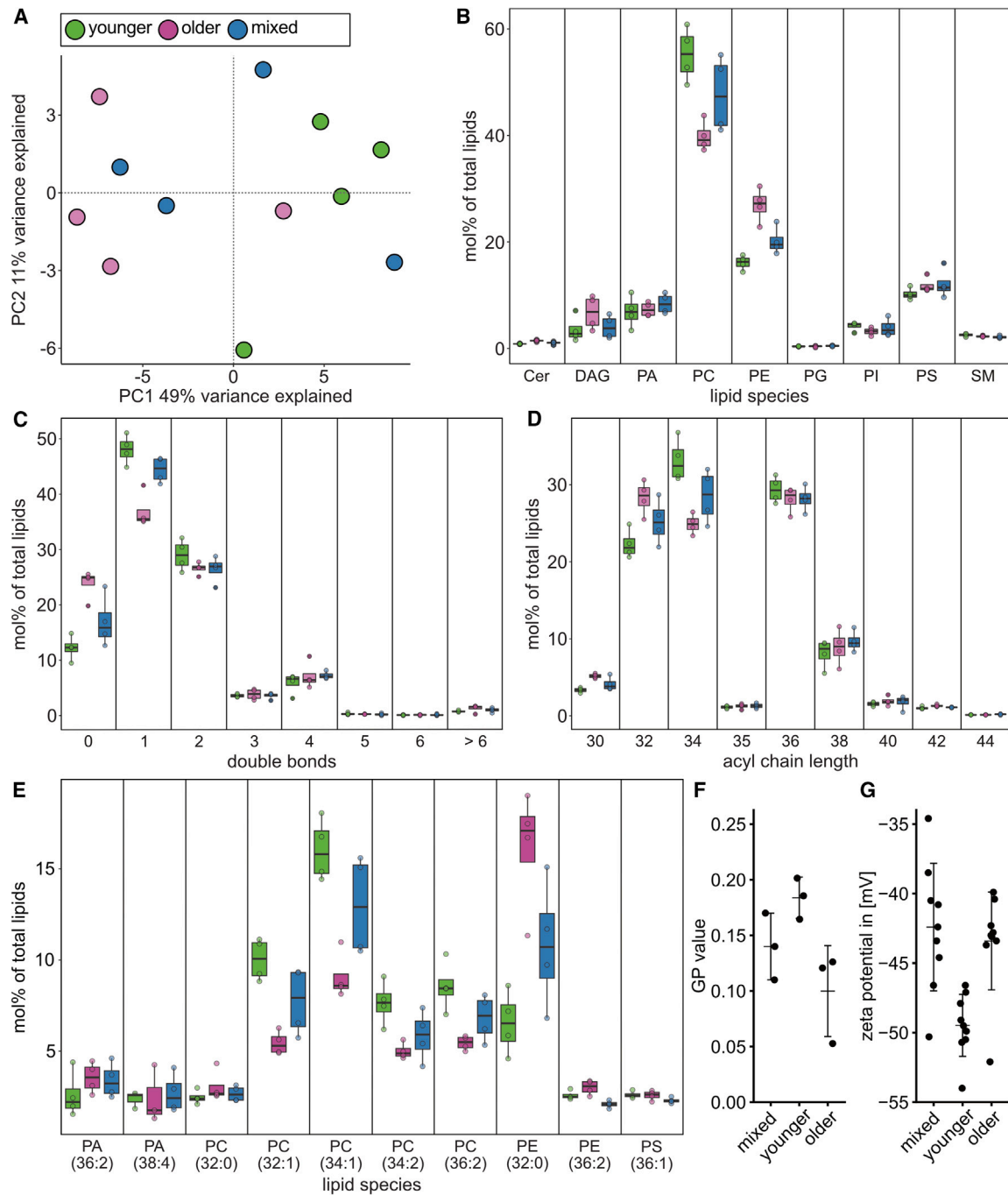


Figure 3. Lipid profile of purified young and old SGs

(A) Principal-component analysis of individual samples of younger (green), older (magenta), and mixed (blue) SGs.

(B) Lipid classes detected in preparations of younger (green), older (magenta), and mixed (blue) SGs. Boxplots are shown for ceramide (Cer), diacylglycerol (DAG), phosphatidic acid (PA), phosphatidylcholine (PC), phosphatidylethanolamine (PE), phosphatidylglycerol (PG), phosphatidylinositol (PI), phosphatidylserine (PS), and sphingomyelin (SM).

(C) Distribution of the number of double bonds identified in lipids from younger (green), older (magenta), and mixed (blue) SGs.

(D) Distribution of acyl chain length identified in lipids from younger (green), older (magenta), and mixed (blue) SGs.

(E) Molar percentage of the total measured lipids for the 10 most abundant lipid species measured.

(F and G) General polarization (GP) (F) and zeta potential values (G) of membranes from mixed, younger, and older SGs.

Shown are measurements from three (F) or four (A–E) independent SG preparations. Data are represented as mean \pm SD.

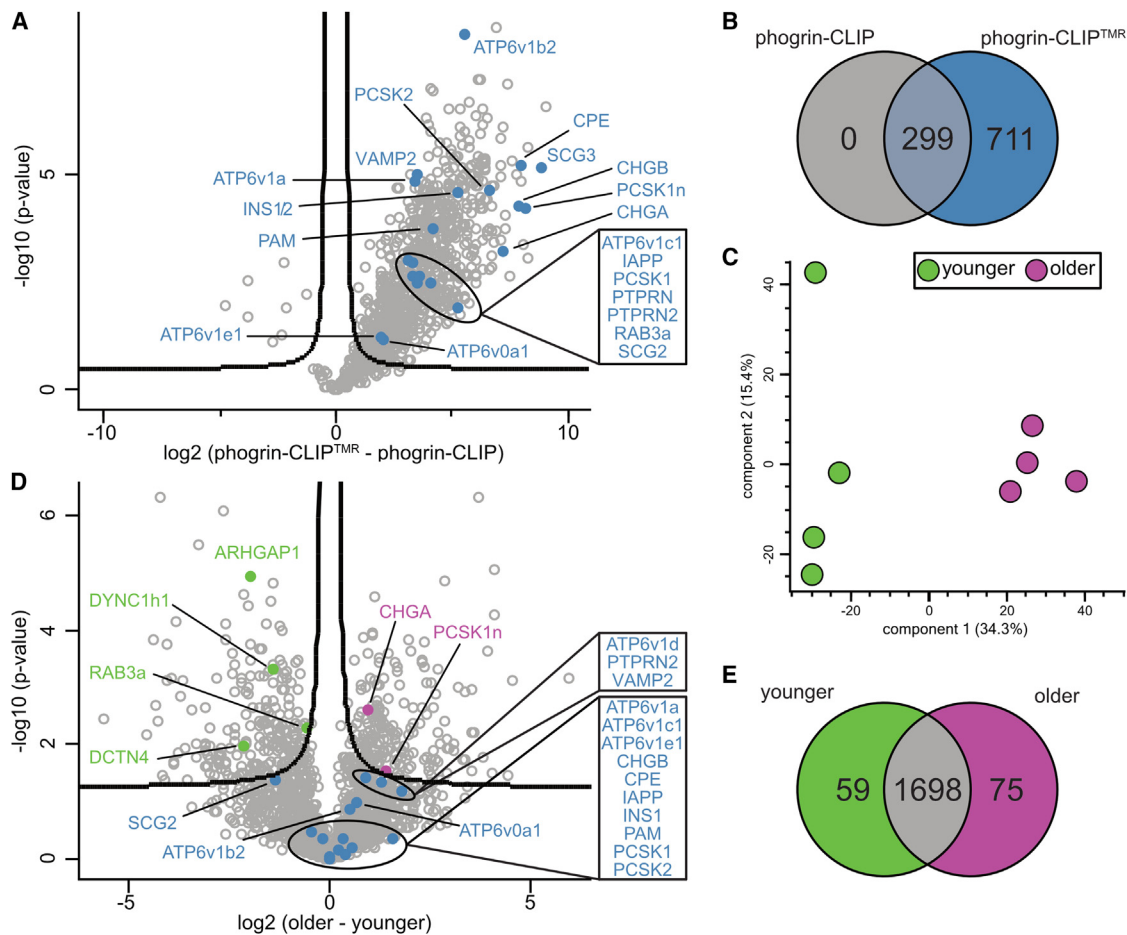


Figure 4. Proteomics characterization of purified SGs

(A) Volcano plot showing proteins significantly enriched in unlabeled (left) and labeled (right) samples, with a false discovery rate (FDR) of 0.05 and S_0 of 0.1. Data represent median values of four independent experiments.

(B) Venn diagram showing the amount of shared or exclusive proteins as identified in (A).

(C) Principal-component analysis of the individual proteomics profiles of younger (green) and older (magenta) SGs.

(D) Volcano plot showing proteins significantly enriched in preparations of younger (left, green) or older (right, magenta) SGs, with an FDR of 0.05 and S_0 of 0.1. SG proteins not significantly changed are shown in blue. Data represent median values of four independent experiments.

(E) Venn diagram showing the amount of shared or exclusive proteins as identified in (D).

younger and older SGs formed well-defined clusters distinct from each other (Figure 4C). Importantly, most known SG proteins, such as INS1/2, IAPP, PC1/3, PC2, and peptidyl-glycine alpha-amidating monooxygenase (PAM), were not enriched in either of the two pools, suggesting that their preparations yielded similar amounts of SGs (Figure 4D). However, the small GTPase RAB3a was enriched in younger SGs, whereas CHGA and ProSaaS were significantly enriched in older SGs (Figure 4D).

When comparing the overall similarities between the samples, we found that 1,698 proteins were shared among the eluates of younger and older SGs, whereas 59 and 75 proteins were exclusive for the eluates of younger or older SGs, respectively (Figure 4E). Significantly enriched were 222 proteins in fractions of younger and 188 in fractions of older SGs (Table S6). Among the shared proteins, cytoplasmic dynein 1 heavy chain 1 (DYNC1h1) as well as its adaptor, dynactin subunit 4 (DCTN4), were enriched on younger SGs (Figure 4D; Table S6). Rho GTPase-activating pro-

tein 1 (ARHGAP1), another cytosolic protein potentially involved in membrane transport, was also significantly enriched on younger SGs. Importantly, the lysosomal markers LAMP1/2, cathepsin A/B, and the endosomal markers RAB7a and RAB11 were not enriched in either fraction, pointing to comparable contamination of the two age-distinct SG pools (Figure S5B).

We further examined proteins exclusive to eluates of either younger or older SGs (Figure S5C; Table S7). Proteins found only in eluates of younger SGs comprised mostly ribosomal (e.g., large ribosomal subunit protein uL4 [RPL4]) or RNA-binding proteins (e.g., eukaryotic translation initiation factor 2 subunit 2 [EIF2s2]), whereas mitochondrial proteins (e.g., GrpE protein homolog 2, mitochondrial [GRPEL2]) were present in eluates of older SGs.

Taken together, these data indicate that most SG proteins, in particular luminal and transmembrane proteins, remain constant during the aging process. However, cytosolic proteins, such as

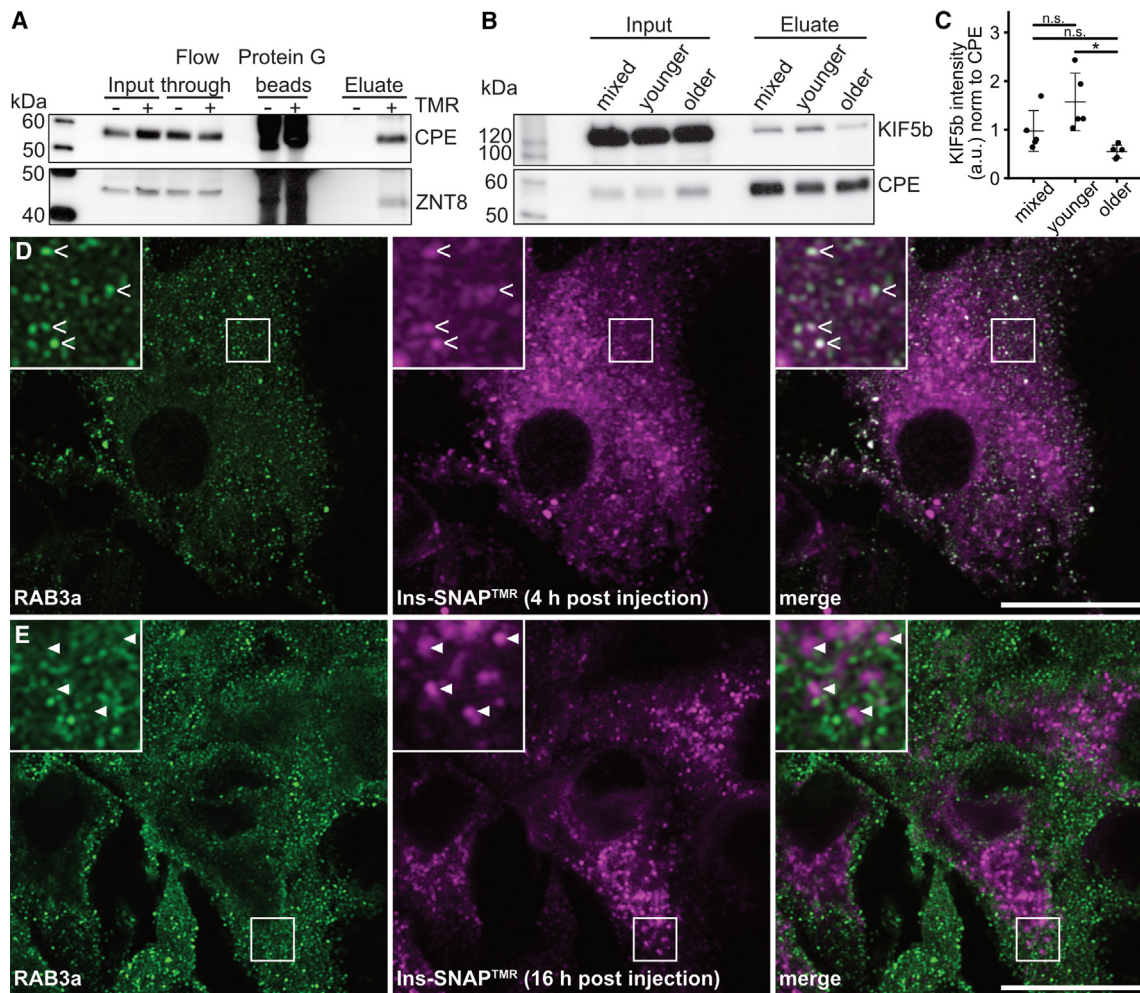


Figure 5. Validation of known SG proteins

(A) Purified mixed SG eluates were probed for ZNT8 and CPE.

(B) SG eluates of mixed, younger, and older SGs were probed for KIF5b and CPE.

(C) Quantification of (B). Data are represented as mean \pm SD. Statistical analysis corresponds to t test; * $p < 0.05$.

(D and E) Representative Airyscan images of pancreatic sections of SOFIA mice labeled *in vivo* with BG-TMR for 4 h (D) or 16 h (E), co-stained for RAB3a. Empty arrowheads highlight co-localizing and filled arrowheads non-co-localizing objects. Scale bars: 10 μ m.

motor proteins or small GTPases, may dynamically interact with SGs of distinct age.

Validation of proteomics data

To validate the association of the identified proteins with SGs, we tested for the known granule transporter zinc transporter 8 (ZNT8), which was not detected by MS but present in immunoblots of isolated SGs (Figure 5A). KIF5b was not classified as significantly enriched in younger or older SGs by MS. However, consistent with its association with SGs⁴⁰ and the increased motility of younger SGs,¹³ we found it to be enriched on younger SGs by immunoblot (Figures 5B, 5C, and S6A). We further immunostained pancreatic sections of *in vivo*-labeled study of insulin aging (SOFIA) mice for RAB3a. Younger SGs of an age of 4 h post BG-TMR injection co-localized well with RAB3a, which had a predominantly peripheral localization (Figure 5D). Older SGs of an age of 16 h post injection

instead were distinct from RAB3a and localized closer to the center of the cells.

Finally, we investigated ARHGAP1, a protein identified as significantly enriched on younger SGs by MS. We probed murine pancreatic sections for the presence of ARHGAP1 and found it to be expressed in islet cells but also in the surrounding exocrine cells (Figure 6A). To validate its preferential association with younger SGs, we labeled INS-1 cells transfected with Ins-SNAP (Figures S6B and S6C) as well as SOFIA mice (Figures 6B and 6C) for younger or older SGs and co-stained for ARHGAP1. We found that ARHGAP1 co-localized both with younger and older SGs. Notably, in both cases, we also observed SGs negative for ARHGAP1. To complement these data, we used immunoelectron microscopy on sections of mouse islets. Immunogold particles were present both on immature and mature SGs, again also showing SGs negative for immunogold (Figure 5E).

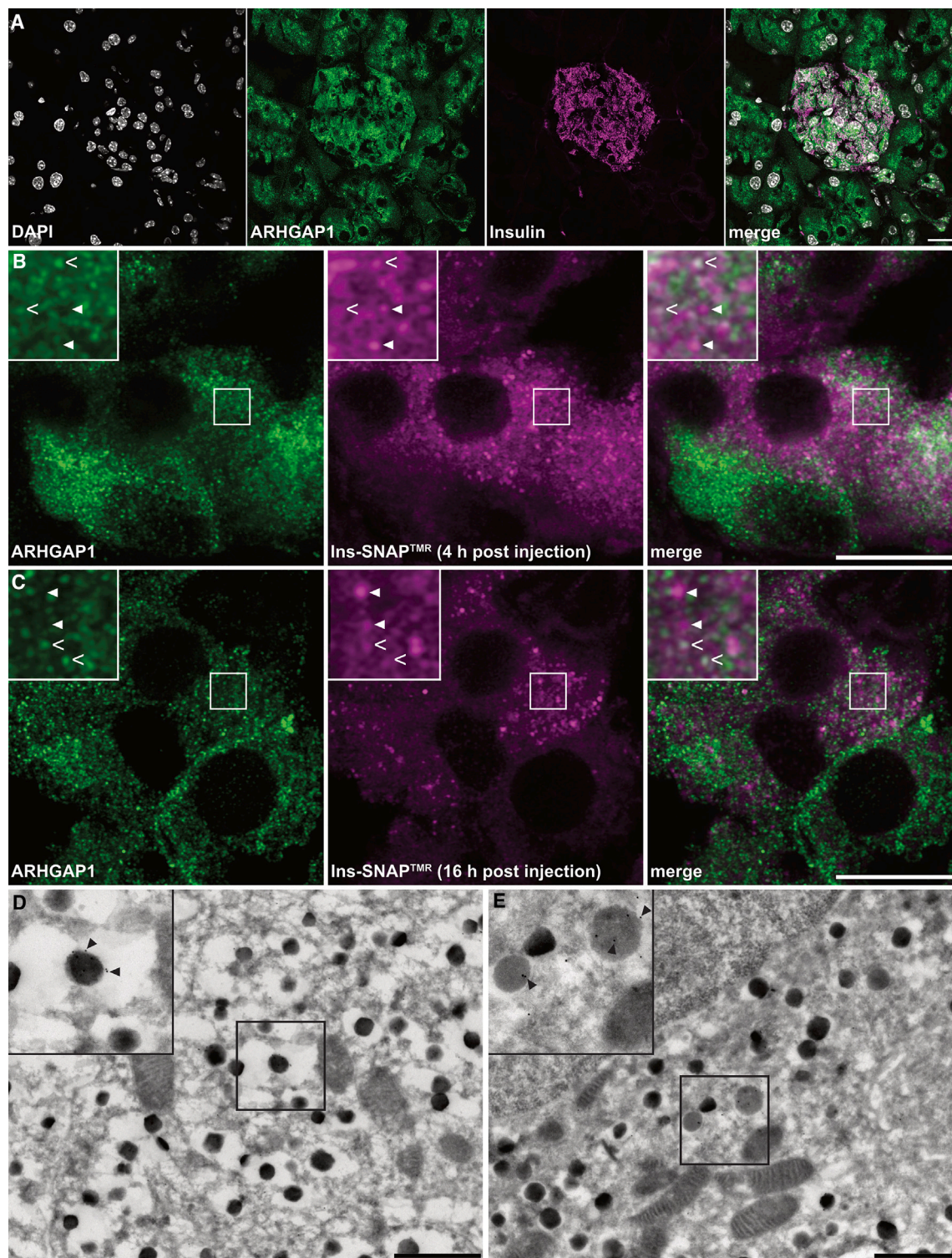


Figure 6. Subcellular localization of ARHGAP1

(A) Confocal image of a mouse pancreatic section stained for nuclei (DAPI), ARHGAP1, and insulin. Scale bar: 20 μ m.

(B and C) Representative Airyscan images of pancreatic sections of SOFIA mice labeled *in vivo* with BG-TMR for 4 h (B) or 16 h (C), co-stained for ARHGAP1. Empty arrowheads highlight co-localizing and filled arrowheads non-co-localizing objects. Scale bars: 10 μ m.

(D and E) Electron micrographs of β cells in isolated mouse islets stained with immunogold for ARHGAP1. Immunogold (filled arrowheads) was detected on dense (D) and less dense, conceivably immature (E) SGs. Scale bars: 1 μ m.

Table 1. Comparison of SG lipids from this study with lipids from previous reports of insulin or chromaffin SGs and islet or cell extracts

Lipid species	Insulin granules			Chromaffin granules			Islet/cell extracts				
	This study	RINm5f ⁴¹	Rat tumor ⁴¹	INS-1 ⁴⁶	Bovine ⁴⁵	Human ⁴⁴	RINm5f ⁴¹	Rat tumor ⁴¹	ob/ob ⁴¹	ob/ob ⁴²	Wistar rat ⁴³
PC	47.7%	39.2%	52.8%	22%	27.5%	16.1%	52.5%	51.2%	49.9%	56%	45.8%
PE	20.2%	12.3%	24.8%	17%	26.6%	29%	18.1%	23.1%	21.2%	11%	20.6%
PI	3.9%	4.1%	7.7%	21%	–	1.1%	6.5%	7.6%	8.6%	12%	8.9%
PS	12.1%	10.8%	3.3%	11%	20.2%	8.5%	3.9%	1.9%	4.1%		14%
SM	2.2%	20.5%	10.7%	10%		16%	7.7%	13.7%	8.4%	8%	10.7%
PA	8.4%	trace	0.9%	–	14.5%	–	trace	trace	3.1%	13%	N/D
CL	N/D	4.1%	0.1%	–	–	–	4.7%	3.2%	0.9%	N/D	N/D
CHOL	N/D	N/D	N/D	–	–	–	N/D	N/D	N/D	N/D	N/D
LPC	N/D	4.2%	4.2%	19%	11.3%	23.1%	1.9%	4.2%	2.7%	N/D	N/D

Data show the contribution of phosphatidylcholine (PC), phosphatidylethanolamine (PE), phosphatidylinositol (PI), phosphatidylserine (PS), sphingomyelin (SM), phosphatidic acid (PA), cardiolipin (CL), cholesterol (CHOL), and lysophosphatidylcholine (LPC). N/D = not detected.

These data indicate that younger SGs are more likely to contain the motor protein KIF5b, consistent with their greater motility, as well as RAB3a, which appeared to be enriched at the cell periphery. ARHGAP1, which has previously not been associated with insulin SGs, was present on a subset of immature, young, and old SGs.

DISCUSSION

The lipidomic and proteomic composition of insulin granules in INS-1 cells

The SG phospholipid levels measured in this study are similar to those reported for insulin granules in RINm5F cells⁴¹ or mouse and rat islet extracts^{42,43} (Table 1) but differ substantially from those observed in chromaffin granules^{44,45} (Table 1). Another study using INS-1 cells⁴⁶ found phospholipids more similar to chromaffin granules (Table 1). These differences may be attributed to the methodology used (solid-phase extraction, gas chromatography [GC]-MS vs. direct infusion), sample purity (differential centrifugation vs. affinity isolation), or even minor differences, like the serum used for cell culture and related variables.

The use of insulinoma cells for phospholipid analyses has been questioned, suggesting that the reduced levels of PA in tumorous rat islets and rat insulinoma RINm5F cells may contribute to reduced glucose-responsive insulin secretion.⁴¹ However, the SG phospholipids of the rat insulinoma INS-1 cells identified here are similar to those of total mouse islet phospholipids, including detectable levels of PA (Table 1). This low-abundance phospholipid acts as a building block for all other phospholipids but is also an important player in cellular signaling, being a recruitment factor for interacting proteins.⁴⁷ For example, PA has been shown to contribute to SG formation at the Golgi apparatus,⁴⁸ docking at the PM,⁴⁹ and, relevant for insulin SG motility, as a binding partner for the motor protein KIF5b on membrane-type matrix metalloproteinase (MT-MMP)-containing exocytotic vesicles.⁵⁰ Unlike RINm5F cells, INS-1 cells are glucose responsive, and, thus, it is possible that differences in PA content on SGs contributes to the distinct secretory properties of various insulinoma cell lines. In addition, the cone-

shaped lipids PA and PE are beneficial for membrane fusion, supporting their importance in exocytosis.^{51–53}

The MS approach used here is not compatible with the measurement of cholesterol, a lipid that is synthesized in the ER and progressively accumulates in membranes along the secretory pathway up to the PM.^{54,55} Cholesterol amounts to 37%–42% of the membrane lipid content of SGs⁵⁶ and greatly influences membrane trafficking at various stages, such as Golgi apparatus export⁵⁷ and SG secretion.^{58,59} Alternative protocols will be required to measure the amount of cholesterol in insulin SGs isolated using our protocol. Although compatible with our MS protocol, we did not detect cardiolipin, a class of lipids specific to the inner mitochondrial membrane, suggesting a lack of considerable mitochondrial membranes in our preparation.

We identified 875 proteins to be significantly enriched in SG fractions, which is likely a vast overestimate of the SG proteome and, thus, reflects the presence of non-SG proteins. Comparative proteomics analyses do not usually rely on absolute but rather on relative quantifications, either with (e.g., stable isotope labeling with amino acids in cell culture [SILAC] or tandem mass tag [TMT]) or without a label. Considering that proteins have unique characteristics influencing tryptic digestion, generation of unique peptides and their detection, direct comparison between individual proteins without standards is difficult. Hence, the relative greater abundance of a protein over the control samples may indicate its enrichment but does not provide information about its absolute amounts. On one hand, advances in MS sensitivity, which greatly enhance the detection of proteins in general,⁶⁰ may amplify this effect. On the other hand, this high sensitivity enabled us to detect well-known SG proteins, like IAPP,^{61,62} which escaped detection in previous MS analysis of isolated SGs.

Several single-pass transmembrane proteins of SGs (e.g., ICA512) were present, but multipass transmembrane proteins, including the well-known and disease-relevant SG protein ZNT8,⁶³ were missed. The low abundance of such multipass transmembrane proteins may hamper the generation of sufficient peptides for unequivocal measurement by MS, hence requiring detection and validation by other means.

It is conceivable that, with the use of different approaches,^{20–22} including this study, the intrinsic SG proteome has by now been

largely characterized and that only spatial, temporal, or stimulus-dependent associations have yet to be discovered.

Differences between younger and older insulin SGs and implications for their exocytosis

Our lipidomics analysis revealed that younger SGs contained higher levels of PC with mono- and di-unsaturated acyl chains (32:1, 34:1, 34:2, and 36:2), whereas older SGs had higher levels of fully saturated PE 32:0 and higher content of DAGs. These variations were associated with a greater fluidity of liposomes formed from lipids extracted from older SGs, as measured by C-Laurdan. This probe, when inserted in membranes, is sensitive to environmental polarity, reporting the local penetration of water, especially in the head group region.^{64,65} The greater abundance of lipids with smaller head groups, like PE and DAG, in older SGs in comparison with younger SGs, which were instead enriched in PC and PI, could explain the elevated membrane fluidity of the older SGs.

Moreover, the liposomes showed overall highly negative zeta potential values, suggesting a high abundance of negatively charged lipids, with the acidic phospholipids PA, PS, and PI being the major contributors. The lower zeta potential of younger SGs suggests a higher abundance of acidic phospholipids. However, the lipidomics data revealed only a minimal increase in PS and slight decrease in PI, indicating that other, non-acidic lipids likely affect the zeta potential. Examples include PE, which has been suggested to influence the protonation state of PA,⁶⁶ polyphosphorylated phosphoinositides, or gangliosides (currently not amenable for shotgun lipidomics). Thus, although the high content of acidic phospholipids (~20 mol %) explains to some extent the overall negative zeta potential, a clear understanding of the difference between younger and older SGs is missing.

Changes in the biophysical properties of SG membranes could influence their ability to recruit cytosolic proteins, and, thus, their traffic, exocytosis, or targeting to intracellular degradation. For example, the RABs 1/5/6 have been shown to specifically insert into negatively charged membranes with lipid packing defects.⁶⁷ Our MS data suggest that younger SGs contain higher levels of RAB3a, which is critical for insulin secretion.^{68,69} RAB3a further co-localized with younger SGs at the cell periphery in islet β cells of *in vivo*-labeled SOFIA mice. This association could be the cause or consequence of a peripheral localization but either way would optimally position younger SGs for secretion. Similarly, the motor proteins dynein and kinesin-1 were enriched on younger SGs and are also relevant for insulin release.⁴⁰ As mentioned above, KIF5b binds to negatively charged membranes, at least *in vitro*.^{50,70} Hence, it is possible that the more negatively charged membrane of younger SGs favors the binding of KIF5b, thus accounting, at least in part, for their greater competence for microtubule-mediated transport.¹³

Taken together, it is possible that the membrane properties are responsible for a preferential association of KIF5b and RAB3a with younger SGs. However, our data do not clarify whether the interaction with RAB3a is established at the time of SG formation at the trans-Golgi network in the perinuclear region or occurs later at the cell periphery. We propose that changes in the membrane of aged SGs lower the association of KIF5b and RAB3a. This, together with translocation of the

SGs within the cell, might explain their reduced propensity for exocytosis relative to younger SGs.³⁻⁶ Due to a lack of reporters and tools for spatial and temporal manipulation of specific lipid species in living cells, this hypothesis may be tested in the future primarily using *in vitro* reconstitution assays.

Our MS data revealed an association of ARHGAP1 with SGs and suggested its enrichment on the younger ones. Our imaging analysis validated this association, but unlike in the case of RAB3a, it indicated that ARHGAP1 can be found on both younger and older SGs as well as on immature SGs in INS-1 cells and in *in vivo*-labeled SOFIA mice. Importantly, not all SGs were positive for ARHGAP1, suggesting that association with SGs is less determined by SG age itself but, rather, through other mechanisms. ARHGAP1 interacts with small GTPases of the Rho family (RhoA, CDC42, and Rac1) and stimulates their GTPase activity, resulting in guanosine triphosphate (GTP) hydrolysis and, thus, in their inactivation. Rho kinases, such as Rac1, play a role in insulin secretion,⁷¹ with the family member CDC42 being implicated in the regulation of the second phase of insulin release.⁷² Considering that we purified SGs under conditions of low glucose, it is possible that ARHGAP1 suppresses insulin secretion facilitated through Rho family members. For example, ARHGAP1 might prevent SGs that are “primed” for exocytosis from being secreted, which would be especially important for immature SGs. Thus, further studies will be necessary to investigate whether and how ARHGAP1 regulates insulin SG traffic and exocytosis, also in relationship to their age.

The differential enrichment of the microtubule motor protein KIF5b, the exocytosis-relevant GTPase RAB3a, and possibly the Rho GTPase-activating ARHGAP1 of aged-distinct SG pools supports a model where younger SGs are preferentially released, whereas older SGs are better poised for degradation by autophagy.^{13,16} Younger SGs may be more prone to direct targeting for lysosomal degradation, such as under conditions of low glucose.⁷³ Comparing younger and older SGs, we mainly found differences in cytosolic but not transmembrane proteins. Selective autophagy of older SGs is therefore likely initiated either by the recruitment of cytosolic factors or the modification of already present proteins. To identify such factors, our protocol could be adapted to conditions inducing autophagy, such as elevated glucose.

The differences in the lipids changing from younger to older SGs was restricted to very few, specific lipid species, indicating a directed process for their exchange or enrichment. Enzymatic exchange of the lipid head groups seems unlikely, as the respective acyl chain lengths and saturation did not match (e.g., PC 34:1 into PE 32:0). One explanation is the transfer of specific lipid species at contact sites between SGs and other membrane organelles, as it has been described to occur at physical proximity sites between the PM and ER, endosomes and ER, or lysosomes and peroxisomes.⁷⁴⁻⁷⁶ This potential lipid transfer might be of a transient nature, and future work will be required to address this possibility.

The molecular mechanisms involved and responsible for SG aging are likely complex and mostly unknown. Changes in the membrane composition, its physical properties, and associated proteins may in part explain the differences in secretion and motility of younger and older SGs. However, more work is required to verify whether these interactions observed *in vitro* occur also *in vivo*.

Limitations of this study and outlook

Isolation of subcellular organelles requires large amounts of starting material, for which immortalized cell lines are usually the preferred source. Although the general composition of organelles in cell lines and primary cells is likely similar, qualitative and quantitative differences may exist. It is therefore possible that proteins expressed in primary cells, but not cell lines, were missed in this study. In addition, cells cultured under defined conditions will inevitably be different from primary cells *in vivo*. For example, lipid metabolism and generation of complex or saturated phospholipids will depend on the presence of the necessary precursors in the culture medium. Although compatible with their detection, we could not identify any phosphorylated phosphatidylinositides (e.g., phosphatidylinositol 4,5-bisphosphate [PIP₂] and phosphatidylinositol 3,4,5-triphosphate [PIP₃]). This could be explained either by their absence or by the low starting material recovered here. In fact, the protocol we describe sacrifices quantity to improve purity. Upscaling is possible, but it would also increase the costs associated with the materials needed. The generation of a transgenic animal model with β -cell-restricted expression of phogrin-CLIP, similar to how we generated transgenic pigs expressing the Ins-SNAP reporter to label and image age-distinct SGs *in vivo*,⁷⁷ might help to address this shortcoming.

Our protocol uses low glucose to minimize the loss of SGs and the recovery of contaminating organelles. However, lack of glucose may also limit the detection of cytosolic factors transiently associated with SG membranes. In the attempt to preserve these interactions, SG secretion could be inhibited pharmacologically or by generating secretion-deficient cell lines, although this may also enhance the rate of intracellular SG degradation.¹⁵

The protocol presented here may further be exploited for metabolomic analyses; e.g., to detect neurotransmitters stored in SGs or peptides resulting from the conversion of prohormones, which are too small to be identified by other means. Other applications are possible, including the characterization of post-translational modifications of SG proteins, the structural analysis of purified SGs by cryoelectron microscopy, or the study of transmembrane proteins in their native environment.

STAR★METHODS

Detailed methods are provided in the online version of this paper and include the following:

- **KEY RESOURCES TABLE**
- **RESOURCE AVAILABILITY**
 - Lead contact
 - Materials availability
 - Data and code availability
- **EXPERIMENTAL MODEL AND STUDY PARTICIPANT DETAILS**
 - INS-1 cells
 - Mouse models
- **METHOD DETAILS**
 - Cell culture and islet isolation
 - Cloning of phogrin-CLIP
 - Generation of BC-Fluorescein(piv)₂

- Age-dependent labeling of SNAP- and CLIP-tagged proteins in cells and *in vivo*
- Sample preparation for fluorescence microscopy, image acquisition and analysis
- Insulin SG purification for SDS-PAGE and Western Blot
- Real-time PCR
- Insulin secretion
- Sample preparation for electron microscopy
- Sample preparation for shotgun lipidomics
- Annotation of lipid species and standard mixture
- Mass spectrometry of lipids
- Lipid identification, quantification, data processing and analysis
- Lipid extraction, GP and zeta potential measurements
- Sample preparation - Proteomics
- Liquid chromatography and mass spectrometry of proteins
- Proteomics raw file processing
- Bioinformatic analysis of proteomics data
- **QUANTIFICATION AND STATISTICAL ANALYSIS**

SUPPLEMENTAL INFORMATION

Supplemental information can be found online at <https://doi.org/10.1016/j.celrep.2024.113836>.

ACKNOWLEDGMENTS

We are grateful to Carla Münster for mouse work and islet isolation as well as Daniela Friedland for help with pancreas sectioning. We thank Bert Nitzsche and Hella Hartmann for advice for SIM and Airyscan imaging, respectively; Maria Heier for technical contributions in developing the purification protocol; Andreas Müller for preliminary electron microscopy tests; and Carolin Wegbrod and Anke Sönmez for cell culture work. We thank the light microscopy facilities of the MPI-CBG Dresden and the Biotec/CRTD Dresden for support with light microscopy. We are also grateful to Bettina Mathes for support with the synthesis of BG-Fluorescein(piv)₂, Howard Davidson for the gift of anti-phogrin antibodies, Iris Lindberg for discussions, and Mrs. Katja Pfriem for administrative support. Work in the Solimena and Coskun labs was supported by the German Center for Diabetes Research (DZD e.V.), which is financed by the German Ministry for Education and Research. Work in the Solimena lab was further supported by funds from the German-Israeli Foundation for Scientific Research and Development (GIF; grant I-1429-201.2/2017) and the Innovative Medicines Initiative 2 Joint Undertaking under grant agreement 115881 (RHAPSODY) and 115797 (INNODIA), which includes financial contributions from the European Union's Framework Program Horizon 2020, the European Federation of Pharmaceutical Industries and Associations (EFPIA), the Swiss State Secretariat for Education, Research, and Innovation under contract 16.0097, as well as JDRF International and The Leona M. and Harry B. Helmsley Charitable Trust. The electron microscopy facility is supported by EFRE (European Fund for Regional Development). M.N. was the recipient of a pre-doctoral fellowship from the Dresden International Graduate School for Biomedicine and Bioengineering (DIGS-BB).

AUTHOR CONTRIBUTIONS

Conceptualization, M.N. and M.S.; methodology, M.N.; validation, M.N., A.-D.B., and M.G.; formal analysis, M.N., M.G., J.V., A.-D.B., P.S., and A.P.; investigation, M.N., A.-D.B., P.S., K.G., M.G., O.T., J.V., and T.K.; resources, J.B. and K.J.; writing – original draft, M.N.; writing – review & editing, M.N., M.G., Ü.C., and M.S.; visualization, M.N. and A.P.; supervision, Ü.C., M.M., and M.S.; funding acquisition, M.N. and M.S.

DECLARATION OF INTERESTS

The authors declare no competing interests.

Received: June 5, 2023

Revised: December 29, 2023

Accepted: February 5, 2024

Published: February 27, 2024

REFERENCES

- Rorsman, P., and Renström, E. (2003). Insulin granule dynamics in pancreatic beta cells. *Diabetologia* 46, 1029–1045. <https://doi.org/10.1007/s00125-003-1153-1>.
- Shibasaki, T., Takahashi, H., Miki, T., Sunaga, Y., Matsumura, K., Yamana, M., Zhang, C., Tamamoto, A., Satoh, T., Miyazaki, J.I., and Seino, S. (2007). Essential role of Epac2/Rap1 signaling in regulation of insulin granule dynamics by cAMP. *Proc. Natl. Acad. Sci. USA* 104, 19333–19338. <https://doi.org/10.1073/pnas.0707054104>.
- Schatz, H., Nierle, C., and Pfeiffer, E.F. (1975). (Pro-)Insulin Biosynthesis and Release of Newly Synthesized (Pro-)Insulin from Isolated Islets of Rat Pancreas in the Presence of Amino Acids and Sulphonylureas. *Eur. J. Clin. Invest.* 5, 477–485. <https://doi.org/10.1111/j.1365-2362.1975.tb00480.x>.
- Gold, G., Gishizky, M.L., and Grodsky, G.M. (1982). Evidence That Glucose “Marks” β Cells Resulting in Preferential Release of Newly Synthesized Insulin. *Science* 218, 56–58. <https://doi.org/10.1126/science.6181562>.
- Halban, P.A. (1982). Differential Rates of Release of Newly Synthesized and of Stored Insulin from Pancreatic Islets. *Endocrinology* 110, 1183–1188. <https://doi.org/10.1210/endo-110-4-1183>.
- Ivanova, A., Kalaidzidis, Y., Dirx, R., Sarov, M., Gerlach, M., Schroth-Diez, B., Müller, A., Liu, Y., Andree, C., Mulligan, B., et al. (2013). Age-Dependent Labeling and Imaging of Insulin Secretory Granules. *Diabetes* 62, 3687–3696. <https://doi.org/10.2337/db12-1819>.
- Kopin, I.J., Breese, G.R., Krauss, K.R., and Weise, V.K. (1968). Selective release of newly synthesized norepinephrine from the cat spleen during sympathetic nerve stimulation. *J. Pharmacol. Exp. Therapeut.* 167, 271–278.
- Collier, B. (1969). The preferential release of newly synthesized transmitter by a sympathetic ganglion. *J. Physiol.* 205, 341–352. <https://doi.org/10.1113/jphysiol.1969.sp008969>.
- Besson, M.J., Cheramy, A., Feltz, P., and Glowinski, J. (1969). RELEASE OF NEWLY SYNTHESIZED DOPAMINE FROM DOPAMINE-CONTAINING TERMINALS IN THE STRIATUM OF THE RAT. *Proc. Natl. Acad. Sci. USA* 62, 741–748. <https://doi.org/10.1073/pnas.62.3.741>.
- Molenaar, P.C., Nickolson, V.J., and Polak, R.L. (1973). Preferential release of newly synthesized 3H-acetylcholine from rat cerebral cortex slices in vitro. *Br. J. Pharmacol.* 47, 97–108. <https://doi.org/10.1111/j.1476-5381.1973.tb08162.x>.
- Macgregor, R.R., Hamilton, J.W., and Cohn, D.V. (1975). The By-pass of Tissue Hormone Stores During the Secretion of Newly Synthesized Parathyroid Hormone^{a,b}. *Endocrinology* 97, 178–188. <https://doi.org/10.1210/endo-97-1-178>.
- Piercy, M., and Shin, S.H. (1981). Newly synthesized prolactin is preferentially secreted by the adenohypophysis in a primary cell culture system. *Mol. Cell. Endocrinol.* 21, 75–84. [https://doi.org/10.1016/0303-7207\(81\)90032-0](https://doi.org/10.1016/0303-7207(81)90032-0).
- Hoboth, P., Müller, A., Ivanova, A., Mziaut, H., Dehghany, J., Sönmez, A., Lachnit, M., Meyer-Hermann, M., Kalaidzidis, Y., and Solimena, M. (2015). Aged insulin granules display reduced microtubule-dependent mobility and are disposed within actin-positive multigranular bodies. *Proc. Natl. Acad. Sci. USA* 112, E667–E676. <https://doi.org/10.1073/pnas.1409542112>.
- Neukam, M., Sönmez, A., and Solimena, M. (2017). FLIM-based pH measurements reveal incretin-induced rejuvenation of aged insulin secretory granules. *Cell Biol.* 10, 1101–174391.
- Marsh, B.J., Soden, C., Alarcón, C., Wicksteed, B.L., Yaekura, K., Costin, A.J., Morgan, G.P., and Rhodes, C.J. (2007). Regulated Autophagy Controls Hormone Content in Secretory-Deficient Pancreatic Endocrine β -Cells. *Mol. Endocrinol.* 21, 2255–2269. <https://doi.org/10.1210/me.2007-0077>.
- Müller, A., Neukam, M., Ivanova, A., Sönmez, A., Münster, C., Kretschmar, S., Kalaidzidis, Y., Kurth, T., Verbavatz, J.-M., and Solimena, M. (2017). A Global Approach for Quantitative Super Resolution and Electron Microscopy on Cryo and Epoxy Sections Using Self-labeling Protein Tags. *Sci. Rep.* 7, 23. <https://doi.org/10.1038/s41598-017-00033-x>.
- Gaus, B., Brüning, D., Hatlapatka, K., and Rustenbeck, I. (2021). Changes in granule mobility and age contribute to changes in insulin secretion after desensitization or rest. *BMJ Open Diabetes Res. Care* 9, e002394. <https://doi.org/10.1136/bmjdr-2021-002394>.
- Duncan, R.R., Greaves, J., Wiegand, U.K., Matskevich, I., Bodammer, G., Apps, D.K., Shipston, M.J., and Chow, R.H. (2003). Functional and spatial segregation of secretory vesicle pools according to vesicle age. *Nature* 422, 176–180. <https://doi.org/10.1038/nature01389>.
- Yau, B., Hays, L., Liang, C., Laybutt, D.R., Thomas, H.E., Gunton, J.E., Williams, L., Hawthorne, W.J., Thorn, P., Rhodes, C.J., and Kebede, M.A. (2020). A fluorescent timer reporter enables sorting of insulin secretory granules by age. *J. Biol. Chem.* 295, 8901–8911. <https://doi.org/10.1074/jbc.RA120.012432>.
- Brunner, Y., Couté, Y., Iezzi, M., Foti, M., Fukuda, M., Hochstrasser, D.F., Wollheim, C.B., and Sanchez, J.-C. (2007). Proteomics Analysis of Insulin Secretory Granules. *Mol. Cell. Proteomics* 6, 1007–1017. <https://doi.org/10.1074/mcp.M600443-MCP200>.
- Hickey, A.J.R., Bradley, J.W.I., Skea, G.L., Middleditch, M.J., Buchanan, C.M., Phillips, A.R.J., and Cooper, G.J.S. (2009). Proteins Associated with Immunopurified Granules from a Model Pancreatic Islet β -Cell System: Proteomic Snapshot of an Endocrine Secretory Granule. *J. Proteome Res.* 8, 178–186. <https://doi.org/10.1021/pr800675k>.
- Schvartz, D., Brunner, Y., Couté, Y., Foti, M., Wollheim, C.B., and Sanchez, J.-C. (2012). Improved characterization of the insulin secretory granule proteomes. *J. Proteomics* 75, 4620–4631. <https://doi.org/10.1016/j.jprot.2012.04.023>.
- Suckale, J., and Solimena, M. (2010). The insulin secretory granule as a signaling hub. *Trends Endocrinol. Metabol.* 21, 599–609. <https://doi.org/10.1016/j.tem.2010.06.003>.
- Huttner, W.B., Schiebler, W., Greengard, P., and De Camilli, P. (1983). Synapsin I (protein I), a nerve terminal-specific phosphoprotein. III. Its association with synaptic vesicles studied in a highly purified synaptic vesicle preparation. *J. Cell Biol.* 96, 1374–1388. <https://doi.org/10.1083/jcb.96.5.1374>.
- Takamori, S., Holt, M., Stenius, K., Lemke, E.A., Grønborg, M., Riedel, D., Urlaub, H., Schenck, S., Brügger, B., Ringler, P., et al. (2006). Molecular Anatomy of a Trafficking Organelle. *Cell* 127, 831–846. <https://doi.org/10.1016/j.cell.2006.10.030>.
- Thomas-Reetz, A., Hell, J.W., During, M.J., Walch-Solimena, C., Jahn, R., and De Camilli, P. (1993). A gamma-aminobutyric acid transporter driven by a proton pump is present in synaptic-like microvesicles of pancreatic beta cells. *Proc. Natl. Acad. Sci. USA* 90, 5317–5321. <https://doi.org/10.1073/pnas.90.11.5317>.
- Walch-Solimena, C., Takei, K., Marek, K.L., Midyett, K., Südhof, T.C., De Camilli, P., and Jahn, R. (1993). Synaptotagmin: a membrane constituent of neuropeptide-containing large dense-core vesicles. *J. Neurosci.* 13, 3895–3903. <https://doi.org/10.1523/JNEUROSCI.13-09-03895.1993>.
- Klemm, R.W., Ejsing, C.S., Surma, M.A., Kaiser, H.-J., Gerl, M.J., Sampaio, J.L., De Robillard, Q., Ferguson, C., Proszynski, T.J., Shevchenko, A., and Simons, K. (2009). Segregation of sphingolipids and sterols during

- formation of secretory vesicles at the trans-Golgi network. *J. Cell Biol.* 185, 601–612. <https://doi.org/10.1083/jcb.200901145>.
29. Wasmeier, C., and Hutton, J.C. (1996). Molecular Cloning of Phogrin, a Protein-tyrosine Phosphatase Homologue Localized to Insulin Secretory Granule Membranes. *J. Biol. Chem.* 271, 18161–18170. <https://doi.org/10.1074/jbc.271.30.18161>.
 30. Gautier, A., Juillerat, A., Heinis, C., Corrêa, I.R., Jr., Kindermann, M., Beaufile, F., and Johnsson, K. (2008). An Engineered Protein Tag for Multiprotein Labeling in Living Cells. *Chem. Biol.* 15, 128–136. <https://doi.org/10.1016/j.chembiol.2008.01.007>.
 31. Davidson, H.W., Rhodes, C.J., and Hutton, J.C. (1988). Intraorganellar calcium and pH control proinsulin cleavage in the pancreatic β cell via two distinct site-specific endopeptidases. *Nature* 333, 93–96. <https://doi.org/10.1038/333093a0>.
 32. Ort, T., Voronov, S., Guo, J., Zawalich, K., Froehner, S.C., Zawalich, W., and Solimena, M. (2001). Dephosphorylation of beta2-syntrophin and Ca²⁺/micro-calpain-mediated cleavage of ICA512 upon stimulation of insulin secretion. *EMBO J.* 20, 4013–4023. <https://doi.org/10.1093/emboj/20.15.4013>.
 33. Trajkovski, M., Mziaut, H., Altkrüger, A., Ouwendijk, J., Knoch, K.-P., Müller, S., and Solimena, M. (2004). Nuclear translocation of an ICA512 cytosolic fragment couples granule exocytosis and insulin expression in β -cells. *J. Cell Biol.* 167, 1063–1074. <https://doi.org/10.1083/jcb.200408172>.
 34. Taraska, J.W., Perrais, D., Ohara-Imaizumi, M., Nagamatsu, S., and Almers, W. (2003). Secretory granules are recaptured largely intact after stimulated exocytosis in cultured endocrine cells. *Proc. Natl. Acad. Sci. USA* 100, 2070–2075. <https://doi.org/10.1073/pnas.0337526100>.
 35. Caromile, L.A., Oganessian, A., Coats, S.A., Seifert, R.A., and Bowen-Pope, D.F. (2010). The Neurosecretory Vesicle Protein Phogrin Functions as a Phosphatidylinositol Phosphatase to Regulate Insulin Secretion. *J. Biol. Chem.* 285, 10487–10496. <https://doi.org/10.1074/jbc.M109.066563>.
 36. Ferri, G., Digiacoio, L., Lavagnino, Z., Occhipinti, M., Bugliani, M., Cappello, V., Caracciolo, G., Marchetti, P., Piston, D.W., and Cardarelli, F. (2019). Insulin secretory granules labelled with phogrin-fluorescent proteins show alterations in size, mobility and responsiveness to glucose stimulation in living β -cells. *Sci. Rep.* 9, 2890. <https://doi.org/10.1038/s41598-019-39329-5>.
 37. Spitzenberger, F., Pietropaolo, S., Verkade, P., Habermann, B., Lacas-Gervais, S., Mziaut, H., Pietropaolo, M., and Solimena, M. (2003). Islet Cell Autoantigen of 69 kDa Is an Arfaptin-related Protein Associated with the Golgi Complex of Insulinoma INS-1 Cells. *J. Biol. Chem.* 278, 26166–26173. <https://doi.org/10.1074/jbc.M213222200>.
 38. Buffa, L., Fuchs, E., Pietropaolo, M., Barr, F., and Solimena, M. (2008). ICA69 is a novel Rab2 effector regulating ER–Golgi trafficking in insulinoma cells. *Eur. J. Cell Biol.* 87, 197–209. <https://doi.org/10.1016/j.ejcb.2007.11.003>.
 39. Kaiser, H.-J., Lingwood, D., Levental, I., Sampaio, J.L., Kalvodova, L., Rajendran, L., and Simons, K. (2009). Order of lipid phases in model and plasma membranes. *Proc. Natl. Acad. Sci. USA* 106, 16645–16650. <https://doi.org/10.1073/pnas.0908987106>.
 40. Varadi, A., Tsuboi, T., Johnson-Cadwell, L.I., Allan, V.J., and Rutter, G.A. (2003). Kinesin I and cytoplasmic dynein orchestrate glucose-stimulated insulin-containing vesicle movements in clonal MIN6 beta-cells. *Biochem. Biophys. Res. Commun.* 311, 272–282. <https://doi.org/10.1016/j.bbrc.2003.09.208>.
 41. Rustenbeck, I., Matthies, A., and Lenzen, S. (1994). Lipid composition of glucose-stimulated pancreatic islets and insulin-secreting tumor cells. *Lipids* 29, 685–692. <https://doi.org/10.1007/BF02538912>.
 42. Fex, G., and Lernmark, A. (1972). Effect of D-glucose on the incorporation of ³²P into phospholipids of mouse pancreatic islets. *FEBS Lett.* 25, 287–291. [https://doi.org/10.1016/0014-5793\(72\)80505-2](https://doi.org/10.1016/0014-5793(72)80505-2).
 43. Díaz, G.B., Cortizo, A.M., García, M.E., and Gagliardino, J.J. (1988). Lipid composition of normal male rat islets. *Lipids* 23, 1125–1128. <https://doi.org/10.1007/BF02535277>.
 44. De Oliveira Filgueiras, O.M., Van Den Bosch, H., Johnson, R.G., Carty, S.E., and Scarpa, A. (1981). Phospholipid composition of some amine storage granules. *FEBS Lett.* 129, 309–313. [https://doi.org/10.1016/0014-5793\(81\)80190-1](https://doi.org/10.1016/0014-5793(81)80190-1).
 45. Balzer, H., and Khan, A.R. (1975). The different fatty acid composition of lecithins in the sacroplasmic reticulum vesicles and the membranes of adrenal chromaffin granules. *Naunyn-Schmiedeberg's Arch. Pharmacol.* 291, 319–333. <https://doi.org/10.1007/BF00501791>.
 46. MacDonald, M.J., Ade, L., Ntambi, J.M., Ansari, I.-U.H., and Stoker, S.W. (2015). Characterization of Phospholipids in Insulin Secretory Granules and Mitochondria in Pancreatic Beta Cells and Their Changes with Glucose Stimulation. *J. Biol. Chem.* 290, 11075–11092. <https://doi.org/10.1074/jbc.M114.628420>.
 47. Tanguy, E., Kassas, N., and Vitale, N. (2018). Protein–Phospholipid Interaction Motifs: A Focus on Phosphatidic Acid. *Biomolecules* 8, 20. <https://doi.org/10.3390/biom8020020>.
 48. Carmon, O., Laguerre, F., Riachy, L., Delestre-Delacour, C., Wang, Q., Tanguy, E., Jeandel, L., Cartier, D., Thahouly, T., Haeberlé, A.M., et al. (2020). Chromogranin A preferential interaction with Golgi phosphatidic acid induces membrane deformation and contributes to secretory granule biogenesis. *Faseb. J.* 34, 6769–6790. <https://doi.org/10.1096/fj.202000074R>.
 49. Tanguy, E., Costé de Bagneaux, P., Kassas, N., Ammar, M.-R., Wang, Q., Haeberlé, A.M., Raheindratsara, J., Fouillen, L., Renard, P.-Y., Montero-Hadjadj, M., et al. (2020). Mono- and Poly-unsaturated Phosphatidic Acid Regulate Distinct Steps of Regulated Exocytosis in Neuroendocrine Cells. *Cell Rep.* 32, 108026. <https://doi.org/10.1016/j.celrep.2020.108026>.
 50. Wang, Z., Zhang, F., He, J., Wu, P., Tay, L.W.R., Cai, M., Nian, W., Weng, Y., Qin, L., Chang, J.T., et al. (2017). Binding of PLD2-Generated Phosphatidic Acid to KIF5B Promotes MT1-MMP Surface Trafficking and Lung Metastasis of Mouse Breast Cancer Cells. *Dev. Cell* 43, 186–197.e7. <https://doi.org/10.1016/j.devcel.2017.09.012>.
 51. François-Martin, C., Bacle, A., Rothman, J.E., Fuchs, P.F.J., and Pincet, F. (2021). Cooperation of Conical and Polyunsaturated Lipids to Regulate Initiation and Processing of Membrane Fusion. *Front. Mol. Biosci.* 8, 763115. <https://doi.org/10.3389/fmolb.2021.763115>.
 52. Joardar, A., Pattnaik, G.P., and Chakraborty, H. (2021). Effect of Phosphatidylethanolamine and Oleic Acid on Membrane Fusion: Phosphatidylethanolamine Circumvents the Classical Stalk Model. *J. Phys. Chem. B* 125, 13192–13202. <https://doi.org/10.1021/acs.jpcc.1c08044>.
 53. Ohki, S., and Ohshima, H. (1985). Divalent cation-induced phosphatidic acid membrane fusion. Effect of ion binding and membrane surface tension. *Biochim. Biophys. Acta* 812, 147–154. [https://doi.org/10.1016/0005-2736\(85\)90532-2](https://doi.org/10.1016/0005-2736(85)90532-2).
 54. van Meer, G., Voelker, D.R., and Feigenson, G.W. (2008). Membrane lipids: where they are and how they behave. *Nat. Rev. Mol. Cell Biol.* 9, 112–124. <https://doi.org/10.1038/nrm2330>.
 55. Ikonen, E., and Olkkonen, V.M. (2023). Intracellular Cholesterol Trafficking. *Cold Spring Harbor Perspect. Biol.* 15, a041404. <https://doi.org/10.1101/cshperspect.a041404>.
 56. Wang, R., Hosaka, M., Han, L., Yokota-Hashimoto, H., Suda, M., Mitsushima, D., Torii, S., and Takeuchi, T. (2006). Molecular probes for sensing the cholesterol composition of subcellular organelle membranes. *Biochim. Biophys. Acta* 1761, 1169–1181. <https://doi.org/10.1016/j.bbailp.2006.06.016>.
 57. Wang, Y., Thiele, C., and Huttner, W.B. (2000). Cholesterol is required for the formation of regulated and constitutive secretory vesicles from the trans-Golgi network. *Traffic* 1, 952–962. <https://doi.org/10.1034/j.1600-0854.2000.011205.x>.

58. Dirkx, R., and Solimena, M. (2012). Cholesterol-enriched membrane rafts and insulin secretion. *J. Diabetes Investig.* 3, 339–346. <https://doi.org/10.1111/j.2040-1124.2012.00200.x>.
59. Sezgin, E., Gutmann, T., Buhl, T., Dirkx, R., Grzybek, M., Coskun, Ü., Solimena, M., Simons, K., Levental, I., and Schwille, P. (2015). Adaptive Lipid Packing and Bioactivity in Membrane Domains. *PLoS One* 10, e0123930. <https://doi.org/10.1371/journal.pone.0123930>.
60. Brunner, A.D., Thielert, M., Vasilopoulou, C., Ammar, C., Coscia, F., Mund, A., Hoerning, O.B., Bache, N., Apalategui, A., Lubeck, M., et al. (2022). Ultra-high sensitivity mass spectrometry quantifies single-cell proteome changes upon perturbation. *Mol. Syst. Biol.* 18, e10798. <https://doi.org/10.15252/msb.202110798>.
61. Westermarck, P., Wernstedt, C., Wilander, E., Hayden, D.W., O'Brien, T.D., and Johnson, K.H. (1987). Amyloid fibrils in human insulinoma and islets of Langerhans of the diabetic cat are derived from a neuro peptide-like protein also present in normal islet cells. *Proc. Natl. Acad. Sci. USA* 84, 3881–3885. <https://doi.org/10.1073/pnas.84.11.3881>.
62. Cooper, G.J., Willis, A.C., Clark, A., Turner, R.C., Sim, R.B., and Reid, K.B. (1987). Purification and characterization of a peptide from amyloid-rich pancreases of type 2 diabetic patients. *Proc. Natl. Acad. Sci. USA* 84, 8628–8632. <https://doi.org/10.1073/pnas.84.23.8628>.
63. Chimienti, F., Devergnas, S., Favier, A., and Seve, M. (2004). Identification and Cloning of a β -Cell-Specific Zinc Transporter, ZnT-8, Localized Into Insulin Secretory Granules. *Diabetes* 53, 2330–2337. <https://doi.org/10.2337/diabetes.53.9.2330>.
64. Dodes Traian, M.M., Flecha, F.L.G., and Levi, V. (2012). Imaging lipid lateral organization in membranes with C-laurdan in a confocal microscope. *J. Lipid Res.* 53, 609–616. <https://doi.org/10.1194/jlr.D021311>.
65. Barucha-Kraszewska, J., Kraszewski, S., and Ramseyer, C. (2013). Will C-Laurdan dethrone Laurdan in fluorescent solvent relaxation techniques for lipid membrane studies? *Langmuir* 29, 1174–1182. <https://doi.org/10.1021/la304235r>.
66. Kooijman, E.E., Carter, K.M., van Laar, E.G., Chupin, V., Burger, K.N.J., and de Kruijff, B. (2005). What makes the bioactive lipids phosphatidic acid and lysophosphatidic acid so special? *Biochemistry* 44, 17007–17015. <https://doi.org/10.1021/bi0518794>.
67. Kulakowski, G., Bousquet, H., Manneville, J.-B., Bassereau, P., Goud, B., and Oesterlin, L.K. (2018). Lipid packing defects and membrane charge control RAB GTPase recruitment. *Traffic* 19, 536–545. <https://doi.org/10.1111/tra.12568>.
68. Regazzi, R., Ravazzola, M., Iezzi, M., Lang, J., Zahraoui, A., Andereggen, E., Morel, P., Takai, Y., and Wollheim, C.B. (1996). Expression, localization and functional role of small GTPases of the Rab3 family in insulin-secreting cells. *J. Cell Sci.* 109, 2265–2273. <https://doi.org/10.1242/jcs.109.9.2265>.
69. Yaekura, K., Julyan, R., Wicksteed, B.L., Hays, L.B., Alarcon, C., Sommers, S., Poitout, V., Baskin, D.G., Wang, Y., Philipson, L.H., and Rhodes, C.J. (2003). Insulin Secretory Deficiency and Glucose Intolerance in Rab3A Null Mice. *J. Biol. Chem.* 278, 9715–9721. <https://doi.org/10.1074/jbc.M211352200>.
70. Kumar, P., Sanghavi, P., Chaudhury, D., and Mallik, R. (2023). Phosphatidic Acid Dependent Recruitment of Microtubule Motors to Spherical Supported Lipid Bilayers for In-vitro Motility Assays. *Cell Biol.* <https://doi.org/10.1101/2023.10.31.564930>.
71. Veluthakal, R., Madathilparambil, S.V., McDonald, P., Olson, L.K., and Kowluru, A. (2009). Regulatory roles for Tiam1, a guanine nucleotide exchange factor for Rac1, in glucose-stimulated insulin secretion in pancreatic beta-cells. *Biochem. Pharmacol.* 77, 101–113. <https://doi.org/10.1016/j.bcp.2008.09.021>.
72. Wang, Z., Oh, E., and Thurmond, D.C. (2007). Glucose-stimulated Cdc42 signaling is essential for the second phase of insulin secretion. *J. Biol. Chem.* 282, 9536–9546. <https://doi.org/10.1074/jbc.M610553200>.
73. Goginashvili, A., Zhang, Z., Erbs, E., Spiegelhalter, C., Kessler, P., Mihlan, M., Pasquier, A., Krupina, K., Schieber, N., Cinque, L., et al. (2015). Insulin granules. Insulin secretory granules control autophagy in pancreatic β cells. *Science* 347, 878–882. <https://doi.org/10.1126/science.aaa2628>.
74. Eisenberg-Bord, M., Shai, N., Schuldiner, M., and Bohnert, M. (2016). A Tether Is a Tether Is a Tether: Tethering at Membrane Contact Sites. *Dev. Cell* 39, 395–409. <https://doi.org/10.1016/j.devcel.2016.10.022>.
75. Saheki, Y., and De Camilli, P. (2017). Endoplasmic Reticulum–Plasma Membrane Contact Sites. *Annu. Rev. Biochem.* 86, 659–684. <https://doi.org/10.1146/annurev-biochem-061516-044932>.
76. Panagiotou, S., Tan, K.W., Nguyen, P.M., Müller, A., Oqua, A.I., Tomas, A., Wendt, A., Eliasson, L., Tengholm, A., Solimena, M., and Idevall-Hagren, O. (2023). OSBP-mediated PI(4)P-cholesterol exchange at endoplasmic reticulum-secretory granule contact sites controls insulin secretion. *Cell Biol.* <https://doi.org/10.1101/2023.02.22.529485>.
77. Kemter, E., Müller, A., Neukam, M., Ivanova, A., Klymiuk, N., Renner, S., Yang, K., Broichhagen, J., Kurome, M., Zakhartchenko, V., et al. (2021). Sequential in vivo labeling of insulin secretory granule pools in *INS* -SNAP transgenic pigs. *Proc. Natl. Acad. Sci. USA* 118, e2107665118. <https://doi.org/10.1073/pnas.2107665118>.
78. Wasmeier, C., Burgos, P.V., Trudeau, T., Davidson, H.W., and Hutton, J.C. (2005). An Extended Tyrosine-Targeting Motif for Endocytosis and Recycling of the Dense-Core Vesicle Membrane Protein Phogrin: Recycling of Phogrin. *Traffic* 6, 474–487. <https://doi.org/10.1111/j.1600-0854.2005.00292.x>.
79. Asfari, M., Janjic, D., Meda, P., Li, G., Halban, P.A., and Wollheim, C.B. (1992). Establishment of 2-mercaptoethanol-dependent differentiated insulin-secreting cell lines. *Endocrinology* 130, 167–178. <https://doi.org/10.1210/endo.130.1.1370150>.
80. Gotoh, M., Maki, T., Kiyozumi, T., Satomi, S., and Monaco, A.P. (1985). An improved method for isolation of mouse pancreatic islets. *Transplantation* 40, 437–438. <https://doi.org/10.1097/00007890-198510000-00018>.
81. R Core Team (2023). R: A language and environment for statistical computing. <https://www.R-project.org/>.
82. Wickham, H. (2016). ggplot2: Elegant Graphics for Data Analysis (Springer International Publishing). <https://doi.org/10.1007/978-3-319-24277-4>.
83. Hermel, J.-M., Dirkx, R., and Solimena, M. (1999). Post-translational modifications of ICA512, a receptor tyrosine phosphatase-like protein of secretory granules: Post-translational modifications of ICA512. *Eur. J. Neurosci.* 11, 2609–2620. <https://doi.org/10.1046/j.1460-9568.1999.00677.x>.
84. Hanker, J.S., Deb, C., Wasserkrug, H.L., and Seligman, A.M. (1966). Staining Tissue for Light and Electron Microscopy by Bridging Metals with Multidentate Ligands. *Science* 152, 1631–1634. <https://doi.org/10.1126/science.152.3729.1631>.
85. Venable, J.H., and Coggeshall, R. (1965). A SIMPLIFIED LEAD CITRATE STAIN FOR USE IN ELECTRON MICROSCOPY. *J. Cell Biol.* 25, 407–408. <https://doi.org/10.1083/jcb.25.2.407>.
86. Tokuyasu, K.T. (1980). Immunocytochemistry on ultrathin frozen sections. *Histochem. J.* 12, 381–403. <https://doi.org/10.1007/BF01011956>.
87. Slot, J.W., and Geuze, H.J. (2007). Cryosectioning and immunolabeling. *Nat. Protoc.* 2, 2480–2491. <https://doi.org/10.1038/nprot.2007.365>.
88. Völkner, M., Wagner, F., Steinheuer, L.M., Carido, M., Kurth, T., Yazbeck, A., Schor, J., Wieneke, S., Ebner, L.J.A., Del Toro Runzer, C., et al. (2022). HBEGF-TNF induce a complex outer retinal pathology with photoreceptor cell extrusion in human organoids. *Nat. Commun.* 13, 6183. <https://doi.org/10.1038/s41467-022-33848-y>.
89. Ejsing, C.S., Sampaio, J.L., Surendranath, V., Duchoslav, E., Ekroos, K., Klemm, R.W., Simons, K., and Shevchenko, A. (2009). Global analysis of the yeast lipidome by quantitative shotgun mass spectrometry. *Proc. Natl. Acad. Sci. USA* 106, 2136–2141. <https://doi.org/10.1073/pnas.0811700106>.
90. Sampaio, J.L., Gerl, M.J., Klose, C., Ejsing, C.S., Beug, H., Simons, K., and Shevchenko, A. (2011). Membrane lipidome of an epithelial cell line. *Proc. Natl. Acad. Sci. USA* 108, 1903–1907. <https://doi.org/10.1073/pnas.1019267108>.

91. Herzog, R., Schwudke, D., Schuhmann, K., Sampaio, J.L., Bornstein, S.R., Schroeder, M., and Shevchenko, A. (2011). A novel informatics concept for high-throughput shotgun lipidomics based on the molecular fragmentation query language. *Genome Biol.* *12*, R8. <https://doi.org/10.1186/gb-2011-12-1-r8>.
92. Herzog, R., Schuhmann, K., Schwudke, D., Sampaio, J.L., Bornstein, S.R., Schroeder, M., and Shevchenko, A. (2012). LipidXplorer: A Software for Consensual Cross-Platform Lipidomics. *PLoS One* *7*, e29851. <https://doi.org/10.1371/journal.pone.0029851>.
93. Kim, H.M., Choo, H.-J., Jung, S.-Y., Ko, Y.-G., Park, W.-H., Jeon, S.-J., Kim, C.H., Joo, T., and Cho, B.R. (2007). A Two-Photon Fluorescent Probe for Lipid Raft Imaging: C-Laurdan. *Chembiochem* *8*, 553–559. <https://doi.org/10.1002/cbic.200700003>.
94. Prianichnikov, N., Koch, H., Koch, S., Lubeck, M., Heilig, R., Brehmer, S., Fischer, R., and Cox, J. (2020). MaxQuant Software for Ion Mobility Enhanced Shotgun Proteomics. *Mol. Cell. Proteomics* *19*, 1058–1069. <https://doi.org/10.1074/mcp.TIR119.001720>.
95. Cox, J., Hein, M.Y., Luber, C.A., Paron, I., Nagaraj, N., and Mann, M. (2014). Accurate Proteome-wide Label-free Quantification by Delayed Normalization and Maximal Peptide Ratio Extraction, Termed MaxLFQ. *Mol. Cell. Proteomics* *13*, 2513–2526. <https://doi.org/10.1074/mcp.M113.031591>.

STAR★METHODS

KEY RESOURCES TABLE

REAGENT or RESOURCE	SOURCE	IDENTIFIER
Antibodies		
Anti-ARHGAP1	Atlas antibodies	AB_1078194
Anti-CANX	BD Transduction	AB_397883
Anti-CHGA	Abcam	AB_726879
Anti-CPE	Sigma Aldrich	AB_2083922
Anti-EEA1	Thermo Scientific	AB_10985824
Anti-Fluorescein	Thermo Scientific	AB_221561
Anti-GM130	BD Transduction	AB_398141
Anti-GST	Santa Cruz	AB_627677
Anti- γ -tubulin	Sigma Aldrich	AB_477584
Anti-HIS	Novagen	AB_10807496
Anti-ICA512	self-raised	N/A
Anti-ICA69	Abcam	AB_1861011
Anti-Insulin	Sigma Aldrich	AB_260137
Anti-LAMP2	Thermo Scientific	AB_2134625
Anti-LAMP2	Thermo Scientific	AB_2533900
Anti-LAMP2	this paper	N/A
Anti-PC2	GeneTex	AB_10623189
Anti-PDI	Enzo Life Sciences	AB_916902
Anti-phogrin	Wasmeier et al. ⁷⁸	N/A
Anti-RAB3a	Synaptic Systems	AB_887770
Anti-SNAP	NEB	AB_10631145
Anti-SYP1	Synaptic Systems	AB_10890165
Anti-TGN38	BD Transduction	AB_10015241
Anti-TRITC	Thermo Scientific	AB_1502299
Chemicals, peptides, and recombinant proteins		
BC-Fluorescein(piv) ₂	this paper (Johannes Broichhagen)	N/A
CLIP-Cell Block	NEB	Cat#S9220
CLIP-Cell TMR-Star	NEB	Cat#S9219S
SNAP-Cell 430	NEB	Cat#S9109S
SNAP-Cell Block	NEB	Cat#S9106S
SNAP-Cell TMR-Star	NEB	Cat#S9105S
Critical commercial assays		
Insulin Ultra-Sensitive Assay kit	Cisbio	Cat#62IN2PEG
Deposited data		
Secretory granule proteomics	this paper	PRIDE: PXD050087
Experimental models: Cell lines		
INS-1	Asfari et al. ⁷⁹	CVCL_0352
mPhogrin-HRV3C-CLIPf C931S INS-1	this paper	N/A
Experimental models: Organisms/strains		
Mouse: C57BL/6NCrl	Charles River Laboratories	IMSR_CRL:027
Mouse: SOFIA	Ivanova et al. ⁶	N/A
Oligonucleotides		
Mouse phogrin cDNA	IMAGE consortium	BC_133678

(Continued on next page)

Continued

REAGENT or RESOURCE	SOURCE	IDENTIFIER
R. norvegicus β -actin F: 5'-CAACGGCTCCGGCATGTGCAAGG-3'	this paper	NM_031144.3
R. norvegicus β -actin R: 5'-TCTTCTCCATATCGTCCCAGTTG-3'	this paper	NM_031144.3
R. norvegicus γ -tubulin F: 5'-CAACAGTCCTGGATGTCATGAGG-3'	this paper	NM_145778.2
R. norvegicus γ -tubulin R: 5'-GGTGTGGTTGGCCATCATGAGC-3'	this paper	NM_145778.2
R. norvegicus phogrin F: 5'-TCCAGACAAAGGAGCAGTTT-3'	this paper	NM_031600.2
R. norvegicus phogrin R: 5'-GAGTCTGAAGGACCCCTTA-3'	this paper	NM_031600.2
Synthetic CLIP F: 5'-CACTCCCCTGGAGGTTTAA-3'	this paper	N/A
Synthetic CLIP R: 5'-ACCCAGACAGTTCAGCTT-3'	this paper	N/A
Recombinant DNA		
pEGFP-mPhogrin-HRV3C-CLIPf C931S	this paper	N/A
Software and algorithms		
ImageJ/FIJI	https://imagej.net/	SCR_003070
LipidXplorer	https://lifs-tools.org/lipidexplorer.html	N/A
Perseus	https://maxquant.net/perseus/	SCR_015753
RStudio	https://www.rstudio.com/	SCR_000432

RESOURCE AVAILABILITY

Lead contact

Further information and requests for resources and reagents should be directed to and will be fulfilled by the lead contact, Michele Solimena (michele.solimena@tu-dresden.de).

Materials availability

pEGFP-mPhogrin-HRV3C-CLIPf C931S and the stably expressing mPhogrin-HRV3C-CLIPf C931S INS-1 cell line were developed as part of this study. The cell line and plasmid will be made freely available upon request and with the completion of applicable Material Transfer Agreements. BC-Fluorescein(piv)₂ was generated for this study and is freely available upon request from Johannes Broichhagen.

Data and code availability

- All data reported in this paper will be shared by the [lead contact](#) upon request. Proteomic raw data have been deposited at PRIDE and are publicly available as of the date of publication. Accession numbers are listed in the key resources table.
- This paper does not report original code.
- Any additional information required to reanalyze the data reported in this work paper is available from the [lead contact](#) upon request.

EXPERIMENTAL MODEL AND STUDY PARTICIPANT DETAILS

INS-1 cells

INS-1 cells (CVCL_0352) were cultured in RPMI-1640 containing 10% FBS, 1 mM Na-pyruvate, 2 mM L-glutamine, 50 μ M 2-mercaptoethanol, 100 U/ml penicillin, 100 μ g/mL streptomycin, 20 mM HEPES at 11 mM glucose in monolayer culture and passaged every 3–4 days. INS-1 cells were derived from male New England Deaconess Hospital (NEDH) rats.

Mouse models

Male C57BL/6NcrJ wildtype mice were obtained from Charles River Laboratories and were 24-week-old at the time of organ harvest for islet isolation. Female C57Bl/6J0laHsd wildtype mice were 9-week-old at the time of organ harvest for pancreas sectioning.

Female SOFIA (*mIns2-SNAP* knockin) reporter mice were described previously⁶ and injected with SNAP-Cell TMR-Star at the age of 12 weeks. All animal protocols were approved by the institutional animal care and use committee at the Faculty of Medicine of TU Dresden and all experiments were conducted in accordance with relevant guidelines and regulations.

METHOD DETAILS

Cell culture and islet isolation

The phogrin-HRV3C-CLIPf line was cultured in standard INS-1 medium (RPMI-1640 containing 10% FBS, 1 mM Na-pyruvate, 2 mM L-glutamine, 50 μ M 2-mercaptoethanol, 100 U/ml penicillin, 100 μ g/mL streptomycin, 20 mM HEPES at 11 mM glucose) in monolayer culture and passaged every 3–4 days.

To maintain the stable integration of phogrin-HRV3C-CLIPf, the medium was supplemented with 350 μ g/mL G-418.

To isolate islets from 24 week old C57BL/6NCRl mice, a solution of RPMI 1640 with 0.5 mg/mL collagenase (Sigma, C9263) and 50 ng/mL DNase I (Roche, 10104159001) was injected into the bile duct followed by enzymatic digest and a discontinuous Ficoll (Cytiva, GE17-0300) density gradient.³⁰ The islets were then cultured in RPMI 1640 (Gibco, 11879) supplemented with 10% FBS (Gibco, A5256701), 5.5 mM glucose, 20 mM HEPES (Roth, 9105.3) and 100 U/ml each penicillin and streptomycin (Sigma, P0781) overnight and picked the next day for downstream analyses.

Cloning of phogrin-CLIP

Mouse phogrin cDNA was PCR-amplified using a plasmid obtained from the IMAGE consortium (clone BC_133678) and CLIPf cDNA was PCR-amplified using a plasmid available (pCLIPf) from NEB. First, full-length phogrin was cloned into a pEGFP-N1 backbone, then full-length CLIPf attached at the C terminus. We inserted an HRV 3C protease cleavage site (LEVLFQGP), flanked by linkers (PGDPWPPLP), between phogrin and CLIPf, resulting in phogrin-linker-HRV3C-linker-CLIPf. Phogrin was mutated (C931S) to abolish phosphatase activity.³⁵ The fusion protein was generated by standard molecular cloning techniques.

Generation of BC-Fluorescein(piv)₂

Solvents for chromatography and reactions were purchased HPLC grade (Sigma-Aldrich, 99.8%, extra dry over molecular sieves). If necessary, solvents were degassed either by freeze-pump-thaw or by bubbling N₂ through the vigorously stirred solution for several minutes. Unless otherwise stated, all other reagents were used without further purification from commercial sources.

LC-MS was performed on a Shimadzu MS2020 connected to a Nexera UHPLC system equipped with a Waters ACQUITY UPLC BEH C18 (1.7 μ m, 50 \times 2.1 mm). Buffer A: 0.1% FA in H₂O Buffer B: acetonitrile. The typical gradient was from 10% B for 0.5 min gradient to 90% B over 4.5 min 90% B for 0.5 min gradient to 99% B over 0.5 min with 1 mL/min flow. Retention times (t_R) are given in minutes (min).

Preparative and analytical RP-HPLC was performed on a Waters e2695 system equipped with a 2998 PDA detector for product collection (at 230 nm) on a Supelco Ascentis C18 HPLC Column (preparative: 5 μ m, 250 \times 21.2 mm; analytical: 5 μ m, 250 \times 10 mm). Buffer A: 0.1% TFA in H₂O Buffer B: acetonitrile. The typical gradient was from 10% B for 5 min gradient to 90% B over 45 min 90% B for 5 min gradient to 99% B over 5 min with 8 mL/min flow (preparative) or 4 mL/min (analytical).

High resolution mass spectrometry was performed using a Bruker maXis II ETD hyphenated with a Shimadzu Nexera system. The instruments were controlled via Bruker's otofControl 4.1 and Hystar 4.1 SR2 (4.1.31.1) software. The acquisition rate was set to 3 Hz and the following source parameters were used for positive mode electrospray ionization: Endplate offset = 500 V; capillary voltage = 3800 V; nebulizer gas pressure = 45 psi; dry gas flow = 10 L/min; dry temperature = 250°C. Transfer, quadrupole and collision cell settings are mass range dependent and were fine-adjusted with consideration of the respective analyte's molecular weight. For internal calibration sodium formate clusters were used. Samples were desalted via fast liquid chromatography. A Supelco Titan C18 UHPLC Column, 1.9 μ m, 80 Å pore size, 20 \times 2.1 mm and a 2 min gradient from 10% to 98% aqueous MeCN with 0.1% FA (H₂O: Carl Roth GmbH + Co. KG ROTISOLV Ultra LC-MS; MeCN: Merck KGaA LiChrosolv Acetonitrile hypergrade for LC-MS; FA - Merck KGaA LiChropur Formic acid 98%–100% for LC-MS) was used for separation. Sample dilution in 10% aqueous MeCN (hypergrade) and injection volumes were chosen depending on the analyte's ionization efficiency. Hence, on-column loadings resulted between 0.25 and 5.0 ng. Automated internal re-calibration and data analysis of the recorded spectra were performed with Bruker's DataAnalysis 4.4 SR1 software.

In an Eppendorf tube, 1.0 equiv. of isomerically pure 3-oxo-3',6'-bis(pivaloyloxy)-3H-spiro[isobenzofuran-1,9'-xanthene]-6-carboxylic acid (20.0 mg, 36.7 μ mol) was dissolved in DMSO (500 μ L) and 4.0 equiv. of DIPEA (19.0 mg, 147 μ mol, 24.3 μ L) before TSTU (13.3 mg, 44.1 μ mol, 1.2 equiv.) was added in one portion. The mixture was incubated for 10 min before 1.5 equiv. of BC-NH₂ (12.7 mg, 55.1 μ mol) were added. The mixture was vortexed and further incubated for 3 h at RT before it was quenched by addition of 20 equiv. of acetic acid and 25 vol% of water. HPLC (MeCN:H₂O+0.1% TFA = 30:70 to 90:10 over 60 min) provided 17.0 mg (22.5 μ mol) of the desired compound as white powder in 61% yield.

Age-dependent labeling of SNAP- and CLIP-tagged proteins in cells and *in vivo*

To label both Insulin-SNAP and phogrin-CLIP, INS-1 cell medium was changed with one containing either non-fluorescent 5 μ M CLIP/SNAP-Cell Block, 2 μ M SNAP-Cell 430, 0.6 μ M CLIP-Cell TMR-Star or 0.6 μ M synthesized CLIP-Fluorescein as indicated in the text. After 30 min the medium was aspirated, the cells washed twice with PBS and replaced by non-modified medium. The cells were washed twice for 30 min and once for 60 min.

To label Ins-SNAP *in vivo*, we injected 30 nmol (benzylguanine) BG-TMR (NEB, S9105S) into the tail vein of each 12-week-old SOFIA mouse.⁶ 4 or 16 h post injection, the mice were sacrificed under isoflurane, the pancreas dissected and fixed in 4% PFA in 0.1 M phosphate buffer.

Sample preparation for fluorescence microscopy, image acquisition and analysis

For SIM imaging, phogrin-CLIP cells were grown on high precision coverslips coated with poly-ornithine until a confluency of about 70–80%. The cells were then labeled with the respective SNAP/CLIP substrates as indicated above. The cells were fixed with 4% PFA for 20 min and permeabilized with 0.1% Triton X-100 for 10 min. The permeabilized cells were blocked for 1 h with 0.2% (fish skin) gelatin solution +0.5% BSA in PBS at RT. The primary antibodies were diluted in blocking solution and the cells labeled for 30 min at RT. Secondary antibody staining was performed similarly for 20 min. For staining of EEA1 (Thermo Scientific, MA5-14794) and LAMP2 (Thermo Scientific, PA1-655) permeabilization was ensured by the presence of 0.1% saponin. The anti-insulin antibody was from Sigma (I-2018) and the anti-SNAP from NEB (P9310S). The coverslips were mounted on glass slides with VectaShield Antifade Mounting Medium and fixed with nail polish. Images were acquired using a DeltaVision OMX SIM with an Olympus Plan-ApochromatN 60× oil objective with an NA of 1.42. Stacks with a z-step size of 125 nm were acquired and reconstructed with the SoftWoRx software package (SoftWoRx, Germiston, South Africa). Staining for ARHGAP1 (Atlas, HPA004689) and RAB3a (Synaptic Systems, 107 111) in INS-1 cells was performed similarly on Triton X-100 permeabilized cells and imaged on a Zeiss LSM980 with a Plan-Apochromat 63x/1.40 Oil objective in Airyscan mode.

For immunostainings of WT or *in vivo* labeled pancreatic sections, dissected pancreata were fixed for 2 h at RT in 4% PFA. The organs were then transferred to 9% sucrose in PBS at 4°C for 2 h, then moved to 18% sucrose in PBS at 4°C overnight. Finally, the pancreas was moved to and stored in 30% sucrose in PBS at 4°C until embedding in TissueTek. Sections were cut at a thickness of 10 μm on a cryostat. The sections were washed twice for 5 min in PBS, then blocked for 30 min with Dako Antibody Diluent (Agilent, S3022) and incubated overnight with primary antibodies against ARHGAP1 (Atlas, HPA004689), RAB3a (Synaptic Systems, 107 111) or insulin (Sigma, I-2018) diluted in antibody diluent at 4°C. Next, the sections were washed three times for 5 min with PBS and incubated for 1 h at RT with secondary antibodies including DAPI. Finally, the sections were washed three times for 5 min with PBS, 15 μL Mowiol were added and covered with a coverslip. Overview images of pancreatic sections were taken on a Nikon Ti2 Eclipse confocal microscope with a Nikon Plan Apo λ 60× Oil objective. High resolution images were acquired on a Zeiss LSM980 with a Plan-Apochromat 63x/1.40 Oil objective in Airyscan mode.

Images were further processed and analyzed using FIJI and R.^{81,82} Contrast was changed for representation purposes. Quantification was performed on background-subtracted raw images.

Insulin SG purification for SDS-PAGE and Western Blot

For isolation of insulin SGs, phogrin-CLIP cells were grown in 175 cm² flasks (typically 3–4 per condition). After labeling as indicated above, the cells were washed once with PBS, then harvested in 10 mL PBS per flask, spun down for 5 min at 1200 rpm, 4°C and the cell pellets resuspended in 500 μL homogenization buffer (250 mM sucrose, 150 mM NaCl, 4 mM HEPES pH 7.4, 1 mM EGTA, 1% Protease Inhibitor Cocktail). For lipidomic and proteomic analyses, 1.5 mM Na₃VO₄ and 1 μM PI-PLC inhibitor U73122 (Tocris) were added to the homogenization buffer. The cell suspensions were homogenized with 12 strokes of a glass homogenizer on ice and the homogenates spun down for 2 min at 1200 rpm, 4°C to remove nuclei and cell debris. From this point on, flasks may be pooled, and numbers indicate amounts/volumes per 175 cm² flask. Aliquots of the postnuclear supernatants (input, 20 μL) were lysed in a lysis buffer and measured by BCA to adjust protein contents of different treatments. Of each condition 10 μg protein was allotted for quality control. Anti-substrate antibodies (anti-TMR from ThermoFisher, A-6397 or anti-Fluorescein from ThermoFisher, A-889; 5 μg per flask) were added to the cell homogenate and rotated for 2 h at 4°C (9 rpm). For each flask, 30 μL Protein G Dynabeads (ThermoFisher) were washed once in 150 μL PBS-T 0.02% and washed another two times with 150 μL HB. The beads were resuspended in 50 μL homogenization buffer and added to the homogenate-antibody suspension and rotated for 1 h at 4°C (9 rpm). The suspension-containing tubes were placed in a magnetic rack and the supernatant transferred in a new tube (flow-through). The same volume as for the input was taken from the flow-through for quality control. The beads were washed three times in 300 μL homogenization buffer per flask for 30 min at 4°C (9 rpm). For three 175 cm² flasks, the beads were resuspended in 400 μL homogenization buffer and 10 μg HRV 3C protease added and rotated overnight. The suspension was placed on a magnetic rack and let it sit for 30–60 s and the supernatants were taken and placed in a new tube in the magnetic rack to remove residual magnetic beads. This step was repeated once. The beads were boiled in an SDS-loading buffer for analysis by Western Blot. To remove potential lysosomal organelles, 2 μg/flask of LAMP2 antibody (Thermo Scientific, 51–2200 or self-made) were added to the eluates and rotated for 3 h at 4°C (9 rpm). For each three flasks 50 μL of Protein G Dynabeads were prepared as above and the eluates transferred to the bead-containing tubes. The tubes were then rotated for 1 h at 4°C (9 rpm), placed on magnetic racks and the eluates transferred to a new tube in the magnetic rack. This step was repeated once and the resulting eluate could be used for Western Blot or other analyses.

Antibodies against ICA512 were self-raised,⁸³ those against phogrin were a kind gift from Howard Davidson (Denver, CO). The Anti-SNAP antibody was from NEB (P9310S), the anti-CHGA from Abcam (ab45179), the anti-PDI from Stressgen (SPA-891), the anti-GST from Santa Cruz (sc-138), the anti-HIS from Novagen (70796-3), the anti-TGN38 from BD Transduction (610898), the anti-PC2 from GeneTex (GTX114625), the anti-CPE from Sigma (AB5314), the anti-γ-tubulin from Sigma (T-6557), the anti-CANX from

BD Transduction (610523), the anti-ICA69 from Abcam (ab81500), the anti-GM130 from BD Transduction (610822) the anti-SYP1 from Synaptic Systems (101011), the anti-EEA1 and the anti-LAMP2 from Thermo Scientific (MA5-14794 and 51-2200, respectively).

Real-time PCR

Real-time PCR was performed using the GoTaq qPCR Master Mix (Promega) according to manufacturer's instructions. Briefly, cDNA from RT reactions was diluted 1:2 in RNase-free water. Triplicate reactions were set up in Semi-skirted 96-Well PCR Plates (0.2 mL) with optical strip caps (Agilent). The PCR reactions were carried out in an AriaMx Real-time PCR System (Agilent). For absolute quantification, serial dilutions of the target sequence cloned into pCRII vectors were used. The results were then normalized by parallel amplification of rat β -actin mRNA. The following primers were used for the detection of rat β -actin (fwd: 5'-CAA CGG CTC CGG CAT GTG CAA GG-3'; rev: 5'-TCT TCT CCA TAT CGT CCC AGT TG-3'), γ -tubulin (fwd: 5'-CAA CAG TCC TGG ATG TCA TGA GG-3'; rev: 5'-GGT GTG GTT GGC CAT CAT GAG C-3'), phogrin (fwd: 5'-TCC AGA CAA AGG AGC AGT TT-3'; rev: 5'-GAG TCT GAA GGA CCC CCT TA-3') and phogrin-CLIP (fwd: 5'-CAC TCC CAC TGG AGG TTT TA-3'; rev: 5'-ACC CAG ACA GTT CCA GCT T-3').

Insulin secretion

Static insulin secretion was measured using an ultrasensitive insulin HTRF kit (Cisbio) according to manufacturer's recommendations.

Sample preparation for electron microscopy

For electron microscopy, insulin SGs were purified as described above. Instead of acetone precipitation, SGs were either used directly for negative staining or fixed for Epon epoxy resin embedding.

For negative staining of purified SGs 5–10 mL of sample was pipetted to a 300-mesh copper grid covered with a thin carbon-coated and glow discharged formvar film and incubated for 10 min to allow SGs to sediment and adhere to the film. Liquid was removed with a piece of filter paper, shortly washed with a drop of water (2x) and stained with 1% uranyl acetate (UA) in water for about 20 s. UA was removed slowly with filter paper and the grid was air dried before inspection.

Protein G bead bound SGs were fixed with a mixture of formaldehyde (FA, prepared from paraformaldehyde pills) and glutaraldehyde (GA) (2% FA/2% GA in 100 mM phosphate buffer), centrifuged, and resuspended in lukewarm agarose (2%). The agarose was cooled down and cut into small blocks for further processing. Samples were postfixed in 2% aqueous OsO₄ solution containing 1.5% potassium ferrocyanide and 2 mM CaCl₂. After washes in water, samples were incubated in 1% thiocarbonylhydrazide, washed again and contrasted in 2% osmium in water for a second time.⁸⁴ Samples were washed in water, *en bloc* contrasted with 1% uranyl acetate/water, washed again in water, dehydrated in a graded series of ethanol, infiltrated in the Epon substitute EMBED 812 (1 + 2, 1 + 1, 2 + 1 Epon/ethanol mixtures, 2x pure Epon), and finally embedded in flat embedding molds. Samples were cured at 65°C in the oven overnight, and ultrathin sections were cut with a Leica UC6 ultramicrotome and collected on formvar-coated slot grids. Sections were contrasted with uranyl acetate and with lead citrate.⁸⁵

For Tokuyasu-cryo-sectioning⁸⁶ and immunogold labeling,^{87,88} the samples were fixed in 4% formaldehyde for 2 h at RT, washed in phosphate buffer, infiltrated stepwise into 10% gelatin (1% for 30 min, 3% for 45 min, 7% for 1 h, 10% for 2 h) at 37°C, cooled down on ice, cut into small blocks, incubated in 2.3 M sucrose/water for 24 h at 4°C, mounted on pins (Leica #16701950), and plunge-frozen in liquid nitrogen. 70–100 nm sections were cut on a Leica UC6+FC6 cryo-ultramicrotome (Leica Microsystems, Wetzlar, Germany) and picked up in methyl cellulose/sucrose (1 part 2% methyl cellulose (MC), Sigma M-6385, 25 cP + 1 part 2.3 M sucrose) using a perfect loop. Ultrathin sections were stained with antibodies against ARHGAP1 (rabbit polyclonal, Atlas HPA004689, 1:20) for immunogold labeling.⁸⁸ Grids were placed upside down on lukewarm PBS in small petri-dishes in a 37°C-incubator for 20 min (3 changes) to remove gelatin, sucrose, and methyl cellulose, then washed with 0.1% glycine/PBS (5 × 1 min), blocked with 1% BSA/PBS (2 × 5 min) and incubated with the primary antibodies for 1 h. Then the sections were washed in PBS (4 × 2 min), and incubated with protein A conjugated to 10 nm gold (1:25, UMC, Utrecht) for 1 h. Finally, the grids were demounted, thoroughly washed in water to get rid of the PBS (10 × 1 min), contrasted with neutral uranyl oxalate (2% uranyl acetate (UA) in 0.15 M oxalic acid, pH 7.0) for 5 min, washed in water and incubated in MC containing 0.4% UA for 5 min. Grids were looped out with a perfect loop, the MC/UA film was reduced to an even thin film and air dried.

All samples were imaged either with a FEI Morgagni 268D (Thermo Fisher Scientific, equipped with a Megaview III camera, SIS-Olympus) or with a Jeol JEM1400 Plus (equipped with a Ruby camera, JEOL) both running at 80 kV acceleration voltage.

Sample preparation for shotgun lipidomics

To extract lipids, we modified a previously reported procedure^{89,90}: SGs were extracted for 15 min on ice, using 10 volumes of CHCl₃/MeOH (10:1 v/v) including the IS mixture used for absolute quantification. Samples were centrifuged (6000 × g, 5 min, 4°C), the organic phase was collected, and the water phase was re-extracted with 8 volumes of CHCl₃/MeOH/acetone/1M HCl (2:1:0.5:0.1 v/v) for 10 min on ice with thorough vortexing. Samples were centrifuged (6000 × g, 5 min, 4°C) and the organic phase was collected, pooled, and afterward evaporated under a nitrogen stream for an additional 6 h. The sample was re-suspended in 30–50 μ L CHCl₃/MeOH (1:2 v/v) for MS analysis. The samples were kept at 4°C during the whole sample preparation and extraction procedure to prevent lipid degradation.

Annotation of lipid species and standard mixture

Glycerophospholipids, DAG and TAG species were annotated as: (lipid class) (number of carbons in all fatty acids)-(number of double bonds in all fatty acids). The internal (IS) standard mixture contained the following: 40 pmol of 1-heptadecanoyl-2-(5Z,8Z,11Z,14Z-eicosatetraenoyl)-sn-glycero-3-phosphocholine (PC 17:0-20:4), 20 pmol of 1-tridecanoyl-sn-glycero-3-phosphocholine (LPC 13:0), 35 pmol of 1-heptadecanoyl-2-(5Z,8Z,11Z,14Z-eicosatetraenoyl)-sn-glycero-3-phospho-L-serine (PS 17:0-20:4), 10 pmol of 1-heptadecanoyl-2-(5Z,8Z,11Z,14Z-eicosatetraenoyl)-sn-glycero-3-phospho-(1'-rac-glycerol) (PG 17:0-20:4), 20 pmol of 1-heptadecanoyl-2-(5Z,8Z,11Z,14Z-eicosatetraenoyl)-sn-glycero-3-phosphate (PA 17:0-20:4), 40 pmol of d5-Diglyceride (DAG D5), 30 pmol of N-(dodecanoyl)-sphing-4-enine-1-phosphocholine (SM C12), 40 pmol of 1-heptadecanoyl-2-(5Z,8Z,11Z,14Z-eicosatetraenoyl)-sn-glycero-3-phosphoethanolamine (PE 17:0-20:4), 30 pmol of N-(dodecanoyl)-sphing-4-enine (CER C12).

Mass spectrometry of lipids

Lipid extract was mixed 1:1 with 7.5 mM ammonium formate solution (dissolved in CHCl₃/MeOH/*i*-ProOH 14:28:58 v/v). For each analysis, 30 μL of samples were loaded onto 96-well plates (Eppendorf, Hamburg) and sealed with aluminum foil. Mass spectrometry analysis was performed on a QExactive instrument equipped with a robotic nanoflow ion source TriVersa NanoMate (Advion Biosciences) using nanoelectrospray chips with a spraying nozzle diameter of 4.1 μm. The ion source was controlled by the Chipsoft 8.3.1 software. The temperature of the ion transfer capillary was 25°C; S-lens RF level was set to 50%. Extract 1 and 2 (10 μL each) were analyzed either in positive and negative ion mode for 1.5 min in a single acquisition at a resolution of $R_{m/z=200} = 140,000$ for FT-MS or in positive and negative ion mode for 38 min in a single acquisition at a resolution of $R_{m/z=200} = 140,000$ for FT-MS and $R_{m/z=200} = 70,000$ for FT-MS/MS. Samples were infused with a backpressure of 1.25 psi and spray voltage of +0.96 kV and -0.96 kV, respectively. To avoid initial spray instability, the delivery time was set to 30 s. Polarity switch from positive to negative ion mode was set at 0.5 resp. 16.5 min after contact closure, followed by a lag of 20 s resp. 30 s after polarity switch for spray stabilization. FT-MS acquisition method starts with positive ion mode for 0.5 min by acquiring the m/z 400–1600 using automated gain control (AGC) of 3×10^6 and maximum ion injection time (IT) of 500 ms. FT-MS/MS + experiments were triggered by an inclusion list for 16 min, including all masses from 400.20 to 1,000.86 with 1 Da intervals and a normalized collision energy (NCE) of 15%. AGC and maximum IT were set to 2×10^4 and 650 ms, respectively. FTMS acquisition in negative ion mode was set for 0.5 min by acquiring the m/z 400–1,600 using AGC of 3×10^6 and IT of 500 ms. FT-MS/MS- experiments were triggered again by an inclusion list for 20.5 min, including all masses from 400.20 to 1,000.86 with 1 Da intervals and NCE of 23%, AGC of 2×10^4 and maximum IT of 650 ms. Target masses for MS/MS were specified in the inclusion list. Raw data are available in [Table S1](#).

Lipid identification, quantification, data processing and analysis

Data were analyzed with an in-house developed lipid identification software based on LipidXplorer.^{91,92} Molecular Fragmentation Query Language (MFQL) queries were compiled for all lipid classes included in the IS mix. Identification was based on combining MS precursor (mass accuracy better than 5 ppm) and MS/MS fragmentation. Data post-processing and normalization were performed using an in-house developed data management system. Only lipid identifications with a signal-to-noise ratio >5 and a signal intensity 5-fold higher than in corresponding blank samples were considered for further data analysis. All downstream analyses were performed in R.⁸¹ Only the lipids measured in 75% or more of the samples were kept. The dataset was log₂-scaled before Principal Component Analysis. The descriptive analysis was performed on the mol %-transformed dataset, i.e., picomole quantities were divided by the sum of the lipids detected in the respective sample and multiplied by 100. Total carbon chain length and double bonds plots result from grouping together all the lipids that present the same number of carbon atoms (total length) or the same number of double bonds (degree of unsaturation) and calculating the mean and standard deviation in each group of samples (younger, older and mixed). Plots were generated using ggplot2.⁸²

Lipid extraction, GP and zeta potential measurements

For characterization of the biophysical properties of the lipids, SG samples were extracted using a two-step extraction protocol (chloroform:methanol 10:1 followed by 2:1).⁸⁹ After each step, the lipid containing organic phase was pooled and dried under a nitrogen stream followed by incubation under vacuum for 4 h to remove organic solvents. The dried lipid film was re-hydrated in 100 μL of water, for 15 min at 600 rpm. To yield unilamellar vesicles (LUVs), samples were subjected to 10 cycles of freezing in liquid nitrogen and subsequent thawing in a heating block at 45°C. The vesicle solution was extruded 21 times through a 100 nm diameter polycarbonate membrane (Whatman Nuclepore, Fisher Scientific, US) using an extrusion kit (Avanti, US). Membrane order of liposomes prepared from SG lipids was assessed by determining C-Laurdan generalized polarization (GP) indices. Liposomes were stained with C-Laurdan⁹³ and incubated for 30 min in the dark at RT. Fluorescence spectra were obtained with a FluoroMax-4 spectrofluorometer (Horiba) equipped with a temperature-controlled Peltier element (Newport) at 23°C. Excitation wavelength was 385 nm. All spectra were recorded thrice, averaged, and background subtracted (non-stained vesicles). The GPs values for C-laurdan were calculated from the following emission bands: (Ch1) 400–460 nm and (Ch2) 470–530 nm, with $GP = I_{Ch1} - I_{Ch2} / I_{Ch1} + I_{Ch2}$.

Zeta potential measurements of LUVs were determined using a ZetaSizer nanoZS instrument (Malvern Panalytical). LUVs were diluted with Milli-Q water to a final 0.1 mg/mL. Prior to measurement, the water was filtered using a PVDF filter with a pore size of 0.22 μm (Millipore). Zeta potential was measured using Dip Cell. After 120 s of equilibration, three consecutive measurements were performed for each sample at 25°C. The zeta potential was determined using Zetasizer Software 7.11.

Sample preparation - Proteomics

Samples used for proteomics analysis were reconstituted in 500 μ L 6M GdmCl, 100 mM Tris-HCl pH 8.5 solubilization buffer. After addition of 10 mM TCEP and 55 mM CAA the samples were boiled for 20 min at 95°C, 800 rpm on a thermoshaker (Eppendorf) followed by sonication at maximum power (Bioruptor) for 10 cycles of 30 s of sonication and 30 s of cooldown each. The sample was briefly spun down and boiled again for 10 min at 95°C, 800 rpm. 1 mL of 100 mM TrisHCl pH 8.5 was added to each sample to dilute the GdmCl molarity below 2 M in total. 10 μ g of Trypsin and LysC each were added to the sample solution followed by overnight digestion at 37°C, 800 rpm on a thermoshaker (Eppendorf). The next day, the sample was acidified to 1% TFA followed by stage-tip cleanup via styrene-divinylbenzene reverse-phase sulfonate (SDB-RPS). Sample liquid was loaded on two 14-gauge stage-tip plugs fixed within a 200 μ L pipette tip. Peptides were cleaned up with 2 \times 100 μ L 99% ddH₂O 1% TFA into 2 \times 100 μ L 99% Iso-propanol 1% TFA at 1200 \times g at RT each using a table-top centrifuge (Eppendorf). Afterward, peptides were eluted with 80% acetonitrile, 5% ammonia, 15% ddH₂O and dried at 30°C in a SpeedVac centrifuge (Eppendorf). Finally, peptides were reconstituted in 4.2 μ L of 2% acetonitrile, 0.1% TFA, 97.9% ddH₂O ready for LC-MS analysis.

Liquid chromatography and mass spectrometry of proteins

LC-MS was performed with an EASY nanoLC 1200 (Thermo Fisher Scientific) coupled online to a modified trapped ion mobility spectrometry quadrupole time-of-flight mass spectrometer (timsTOF Pro, Bruker Daltonik) via nano-electrospray ion source (Captive spray, Bruker Daltonik).⁶⁰ Peptides were loaded on a 50 cm in-house-packed HPLC-column (75 μ m inner diameter packed with 1.9 μ m ReproSil-Pur C18-AQ silica beads, Dr. Maisch). Sample analytes were separated using a linear 120 min gradient from 3% to 30% buffer B in 95 min followed by an increase to 60% for 5 min, and by a 5 min wash at 95% buffer B at 300 nL/min (buffer A: 0.1% formic acid, 99.9% ddH₂O; buffer B: 0.1% formic acid, 80% CAN, 19.9% ddH₂O). The column temperature was kept at 60°C by an in-house-manufactured oven.

Data were acquired in data-dependent PASEF mode with 1 MS1 survey TIMS-MS and 10 PASEF MS/MS scans per acquisition cycle. Ion accumulation and ramp time in the dual TIMS analyser was set to 100 m each and we analyzed the ion mobility range from 1/K0 = 1.6 Vs. cm⁻² to 0.6 Vs. cm⁻². Precursor ions for MS/MS analysis were isolated with 2Th windows for $m/z < 700$ and 3Th for $m/z > 700$ in a total m/z range of 100–1,700 by synchronizing quadrupole switching events with the precursor elution profile from the TIMS device. The collision energy was lowered linearly as a function of increasing mobility starting from 59 eV at 1/K0 = 1.6 VS cm⁻² to 20 eV at 1/K0 = 0.6 Vs. cm⁻². Singly charged precursor ions were excluded with a polygon filter (otof control, Bruker Daltonik). Precursors for MS/MS were picked at an intensity threshold of 2,500 a.u. and resequenced until reaching a 'target value' of 20,000 a.u., considering a dynamic exclusion of 40 s of elution.

Proteomics raw file processing

Raw files were searched against the rat UniProt databases UP000002494_10116.fa and UP000002494_10116_additional.fa with MaxQuant (v.1.6.7), which extracts features from four-dimensional isotope patterns and associated MS/MS spectra.⁹⁴ FDRs were controlled at 1% both on peptide spectral match (PSM) and protein level. Peptides with a minimum length of seven amino acids were considered for the search including *N*-terminal acetylation and methionine oxidation as variable modifications and cysteine carbamidomethylation as fixed modification, while limiting the maximum peptide mass to 4,600 Da. Enzyme specificity was set to trypsin cleaving carboxy terminal to arginine and lysine. A maximum of two missed cleavages were allowed. Maximum precursor and fragment ion mass tolerance were searched as default for TIMS-DDA data, while the main search peptide tolerance was set to 20 ppm. The median absolute mass deviation for the data was less than one ppm. Label-free quantification was performed with the MaxLFQ algorithm and a minimum ratio count of one.⁹⁵

Bioinformatic analysis of proteomics data

Proteomic data was analyzed using Perseus (v.1.6.7.0). Reverse database, contaminant, and only by site modification identifications were removed from the dataset. Median values were calculated for technical replicates and log₂-transformed. The data were then filtered for at least 75% completeness per group. Missing values were then imputed from a data table specific normal distribution estimate with a downshift of 1.8 and a width of 0.3 SD. Samples of unlabeled and labeled SGs, as well as younger and older SGs were tested for differences in their medians using a permutation-based two-sided Student's *t*-test with 250 iterations, an FDR of 0.05 and an S0 of 0.1. The data was presented as volcano plots. Principal component analysis was performed for samples of younger and older SGs to visualize data reproducibility and variability. The mass spectrometry proteomics data have been deposited to the ProteomeXchange Consortium via the PRIDE partner repository with the dataset identifier PXD050087.

QUANTIFICATION AND STATISTICAL ANALYSIS

Throughout the manuscript, all error bars represent the standard deviation (SD) and a two-tailed *t* test was employed to determine statistical significance. Statistical significance values (*p* values) were reported in the figure legends with **p* < 0.05, ***p* < 0.01, ****p* < 0.001 and n.s. as not significant. Statistical tests were implemented in R. Western blot bands were quantified from the same image/exposure using ImageJ/FIJI (a.u.) and KIF5b intensity normalized to corresponding CPH intensities (a.u.). Lipidomic data were quantified using LipidXplorer and R, and proteomic data using Perseus.